RI 9447

REPORT OF INVESTIGATIONS/1993

Estimation of Shear Strength Using Fractals as a Measure of Rock Fracture Roughness

By P. C. McWilliams, J. C. Kerkering, and S. M. Miller

UNITED STATES DEPARTMENT OF THE INTERIOR

BUREAU OF MINES

Report of Investigations 9447

Estimation of Shear Strength Using Fractals as a Measure of Rock Fracture Roughness

By P. C. McWilliams, J. C. Kerkering, and S. M. Miller

UNITED STATES DEPARTMENT OF THE INTERIOR
Bruce Babbitt, Secretary

BUREAU OF MINES

Library of Congress Cataloging in Publication Data:

McWilliams, P. C. (Paul C.)

Estimation of shear strength using fractals as a measure of rock fracture roughness / by P.C. McWilliams, J.C. Kerkering, and S.M. Miller.

p. cm. — (Report of investigations; 9447)

Includes bibliographical references (p. 25).

Supt. of Docs. no.: I 28.23:9447.

1. Rocks—Fracture. 2. Rock mechanics. I. Kerkering, J. C. (John C.). II. Miller, S. M. (Stanley M.). III. Title. IV. Series: Report of investigations (United States. Bureau of Mines); 9447.

TN23.U43 [TA706] 622 s—dc20 [622'.28] 92-23708 CIP

CONTENTS

ILLUSTRATIONS

ILLUSTRATIONS—Continued

TABLES

UNIT OF MEASURE ABBREVIATIONS USED IN THIS REPORT

cm	centimeter	mm^2	square millimeter
c/mm	cycle per millimeter	μm	micrometer
ft	foot	mm/min	millimeter per minute
in	inch	mt/m^2	metric ton per square meter
kN	kilonewton	pct	percent
m	meter	s	second
mm	millimeter		

ESTIMATION OF SHEAR STRENGTH USING FRACTALS AS A MEASURE OF ROCK FRACTURE ROUGHNESS

By P. C. McWilliams,[1] J. C. Kerkering,[2] and S. M. Miller[3]

ABSTRACT

Researchers at the U.S. Bureau of Mines investigated the use of close-range photogrammetry and subsequent stereo digitizing to obtain data from rock fracture roughness profiles. The photogrammetric process yielded results that were acceptable but somewhat inferior to those obtained by a mechanical profilometer. On the basis of this study, further pursuit of photogrammetry as a data collection method in mining is proposed. Fractal geometry was investigated as a means of measuring the roughness of rock fracture profiles. Four fractal algorithms were used: divider method, modified divider method, box method, and spectral method. A comparison of the methods gave ambiguous results. Brown's modified divider method provided the best means of obtaining the fractal dimension. Shear strength estimates were obtained using the parameters of the modified divider method and Myers' Z_2 measure. Because of differences in results when comparing the different ways of obtaining the fractal dimension, future users of fractals in studies of rock fractures are advised to cross-check their results carefully.

[1]Mathematical statistician (retired), Spokane Research Center, U.S. Bureau of Mines, Spokane, WA.
[2]Mathematician, Spokane Research Center.
[3]Mining engineer, Spokane Research Center, and professor of geological engineering, University of Idaho, Moscow, ID.

INTRODUCTION

As part of its continuing efforts to characterize rock masses for enhanced design of mine openings, researchers at the U.S. Bureau of Mines studied rock fracture roughness and its influence on structural behavior. The original goal of this endeavor was to predict the shear strength of natural rock fractures as a function of two variables—fracture roughness and fracture hardness. As is often the case in research, two topics were of special significance to the Bureau researchers.

First, close-range photogrammetry and subsequent stereo digitizing were used as the data-collecting method. This method was contrasted with the more conventional approach of using a mechanical profilometer to collect information about a rock surface profile. The primary motivation for using photogrammetry was that large amounts of information are required for the work. In addition, photogrammetry has potential as a data-gathering procedure in the field, both above and below ground.

Second, fractal geometry [see Mandelbrot report (*33*)][4] was proposed as a means of determining the roughness of rock surface profiles. It was hoped that by using fractal geometry, investigators could move away from the qualitative and subjective techniques presently used to obtain rock surface profiles, which originated with Barton (*7-8*) in 1973. However, the fractal methods did not prove to be a panacea for the problems encountered in quantifying roughness; rather, the ambiguities of the fractal algorithms became a topic of considerable research interest. Furthermore, since the inception of this work, the scientific community's attitude toward applicability of fractal methods has varied considerably and currently tilts in a more skeptical direction.

This Report of Investigations (RI) endeavors to address three directly related topics: the photogrammetric data collection process, use of fractal geometry to describe surface roughness, and a procedure to estimate rock shear strength using roughness and hardness as input variables.

ACKNOWLEDGMENTS

The authors wish to thank the following people for their contributions to this RI: William Durham of Lawrence Livermore Laboratories, Livermore, CA, for conducting precise profilometer measurements that were used in evaluating photogrammetry as a data-collecting technique; Paul Germain of the Centre de Technologie Noranda, Pointe Claire, QU, for providing additional rock roughness data that were used in evaluating fractal computation methods; and Steven Brown of Sandia Laboratories, Sandia, NM, for sharing his insights into the nature of fractals and methods of computing the fractal dimension.

PHOTOGRAMMETRY

This project required a large number of x, y, z measurements[5] on the natural fracture surfaces of rocks so that a quantitative roughness measurement for a given surface could be formulated. Traditionally, the way to generate data for these measurements has been to use a mechanical profilometer. This instrument has a stylus that runs on x-y axes and measures the height of the surface along a given x-y profile. Height readings along the profile are taken at prescribed intervals (usually every 0.05 mm) by a probe that registers differences in voltage. Such an instrument can be quite accurate and reliable.

The mechanical profilometer, however, does have limitations. First, it is rather large, and therefore it is not easily portable. Second, it requires a reliable power source. Third, it can usually measure only small specimens (up to a maximum of a foot square). Fourth, the rock surface must be small enough and of such a shape to fit on the profilometer bed.

These requirements make a typical mechanical profilometer cumbersome for field work, where the fracture surfaces must be measured in situ. Because some faces are up to 4 m across and can be either vertical or inclined, it is difficult to attach a mechanical profilometer. Consequently, an alternative data-recording device was sought that would be portable and yet would be as accurate as a mechanical profilometer. For these reasons, photogrammetry was investigated as being more usable than a profilometer for gathering data on rock fracture surfaces.

Advances in computers and photogrammetry during the last decade now make it possible to collect, reduce, and display digital elevation data efficiently at distances ranging

[4]Italic numbers in parentheses refer to items in the list of references preceding the appendixes at the end of this report.

[5]Throughout this report, the z-axis represents the height of a data point with a base value in the x-y plane. Thus, all two-dimensional profiles have the z-coordinate as the dependent variable and either the x-coordinate or the y-coordinate as the independent variable. All profiles are read perpendicular to either the x-axis or the y-axis. In three dimensions, z = f(x,y).

from several centimeters to many meters. Such technology could provide a workable new approach to measuring rock fracture roughness, particularly with regard to field situations where a wide range of fracture sizes are present. Because this technique relies on photographic stereo pairs, equipment is portable; a permanent record of the entire area of interest on the fracture surface (not just selected traces) is obtained; and the typically cumbersome tasks of rock sample collection and/or instrument setup are avoided. An additional benefit is that digitized elevations can be obtained from a pair of photographs by using a stereo analytic plotter in conjunction with a data acquisition system and a microcomputer.

Thus, the preferred means of data collecting was close-range photogrammetry. First, however, it was necessary to determine that results from this method were as good or better than those obtainable through the use of a mechanical profilometer. To this end, a comparative trace study and an accuracy and precision analysis were conducted.

Photogrammetry is more thoroughly discussed in appendixes A and B. Appendix A is a detailed description of the procedures used in characterizing rock surfaces using close-range photogrammetry. Appendix B is a comparative evaluation of the use of close-range photogrammetry and a mechanical profilometer for data gathering.

FRACTAL GEOMETRY AND ROCK FRACTURE ROUGHNESS

INTRODUCTION

In deriving his Q-statistic for rock mass classification, Barton (*7*) identified rock fracture roughness as an influential variable. A numerical description of the roughness of a rock fracture surface is essential to the estimation of shear strength, dilatancy, and stiffness of the fracture. In this context, the term "fracture" refers to any semiplanar discontinuity in a rock mass (e.g., joint, bedding plane, fault). In engineering practice, the most commonly used measure of roughness is the joint roughness coefficient (JRC) proposed by Barton (*7*) and adopted by the International Society for Rock Mechanics (*26*). This coefficient ranges in value from 0 to 20 and is estimated either by visual matching of surface profiles with "standard" profiles (fig. 1) or by back calculation using peak shear strength and basic friction angle (obtained from direct-shear tests) in conjunction with joint-wall compressive strength. The first approach is highly subjective, while the second has little practical merit because roughness should preferably be used to predict shear strength, not vice versa.

Since Barton's early work (*7*), other scientists have addressed the problem of quantifying his subjective roughness profiles. Ferrero and Giani (*21*) used a geostatistical approach in which variograms were employed as a means of expressing Barton's profiles. Lee, Carr, Barr, and Haas (*31*) used the divider method to establish corresponding fractal dimensions for Barton's 10 profiles. The JRC was then expressed as a second-degree polynomial with the fractal dimension as the independent variable.

At the time this project was started, fractal geometry (*32*) was considered to be a most promising way of describing geometric configurations. In recent years, investigators have attempted to apply fractal geometry to objective descriptions of rock fracture surfaces (*3, 10, 15*). Such work relies on the assumption that natural rock fracture surfaces can be represented by self-affine fractal models, which seem to be more generally applicable to geologic phenomena than self-similar fractal models. In essence, a self-similar fractal is a geometric feature that retains its statistical properties (statistical moments, to be more precise) through various magnifications. That is, the visual and statistical appearances of the feature are similar at all scales of magnification. In contrast, self-affine fractals remain statistically similar only if they are scaled differently in different directions. Examples include the x- or y-coordinate of two-dimensional Brownian motion plotted as a function of time, and surface roughness profiles in which elevation is plotted as a function of horizontal distance (*12*). The fractal dimension D of such self-affine fractals has a value between the topological dimensions of 1 and 2; values of 1.0 to 1.5 are commonly obtained for rock fracture profiles. Thus, D is potentially an appealing measure of surface roughness because it is a single value that is independent of scale.

A literature search revealed four common methods for calculating fractal dimensions of roughness profiles: divider, or yardstick, method; modified divider method; box method; and spectral method. To evaluate these methods, roughness profiles were obtained from three natural fractures, each in a different rock type, using close-range photogrammetry and stereo digitizing. Fractal dimensions and other roughness measures were computed for the profiles and then evaluated and compared.

ROUGHNESS PROFILES

The three rock types studied were basalt, gneiss, and quartzite. The rock specimens were approximately 8 cm on a side, making the roughness profiles 6 to 7 cm long. Ten parallel roughness profiles were digitized in each of two directions, identified as the x- and y-directions. Thus, 20 profiles were obtained from each specimen, making a total of 60 profiles. The regular digitizing interval was

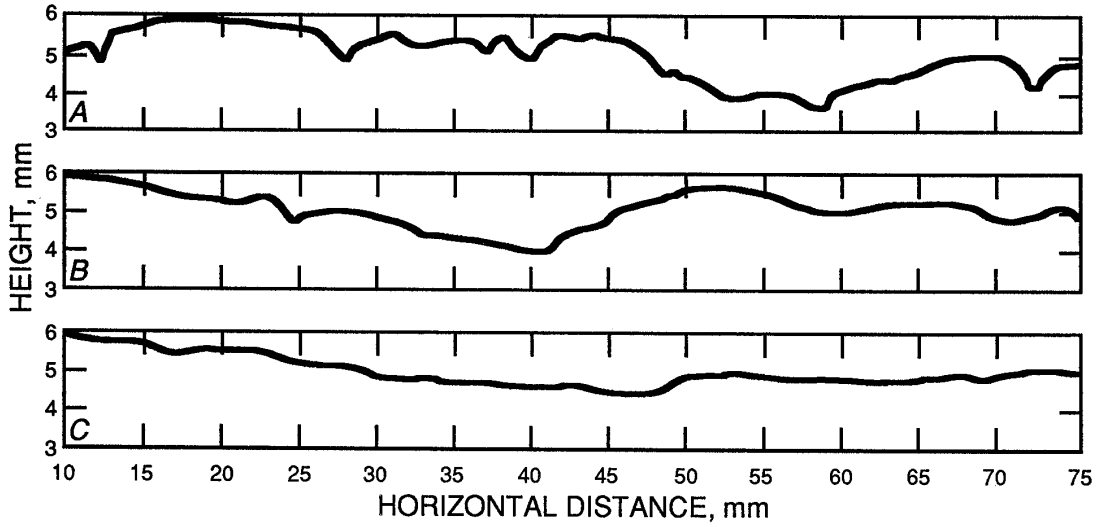

Figure 1.—Examples of fracture roughness profiles. *A*, Basalt; *B*, gneiss; and *C*, quartzite.

approximately 0.052 mm, producing about 1,000 observations in the x-direction and 1,300 observations in the y-direction.

Examples of the roughness profiles are shown in figure 1. In general, a visual assessment of the entire set of profiles indicated that the quartzite fracture was the smoothest of the three, followed by the gneiss fracture, then the basalt fracture. Furthermore, some anisotropy in roughness was observed, especially for the gneiss fracture, where most of the x-profiles appeared smoother than the y-profiles.

COMPUTATIONAL METHODS FOR ESTIMATING FRACTAL DIMENSIONS

Of the four methods used to calculate fractal dimensions of the roughness profiles, the divider and box methods rely on a deterministic approach, while the spectral method relies on a stochastic approach. The deterministic methods are illustrated in figure 2 and are described in more detail below.

Divider Method

The divider, or yardstick, method is best visualized by considering a pair of dividers set to a particular span and then "walked" along the roughness profile. The number of divider spans (yardsticks) required to cover the entire profile is counted and then multiplied by the length of the divider span to give an estimate of the profile length. The divider span is set to another value, and the process is repeated several times to produce a discrete relationship between divider span and profile length. The two are related linearly in log-log space according to the expression

$$\log(L) = A + (1 - D)\log(r),$$

where L = estimated profile length,

A = y-intercept,

and r = divider span [adapted from Feder (*20*)].

Thus, slope b of the log-log plot = 1 - D or D = 1 - b.

Modified Divider Method

A modified divider method proposed by Brown (*12*) consists of using horizontal divider spans (x-increments) rather than walking the dividers along the profile. Thus, the incremental lengths or segments along the profile from x_i to $x_i + 1$ are summed to obtain the total estimated profile length for each given x-increment, which is denoted as r for this case. The above log-log relationship holds, where r = x-increment and D = 1 - b = slope of the log-log plot.

Box Method

Rather than use divider spans as the counting instrument, the box method relies on small rectangular boxes. A box size is selected, which establishes a regular grid, and then the number of such boxes needed to cover

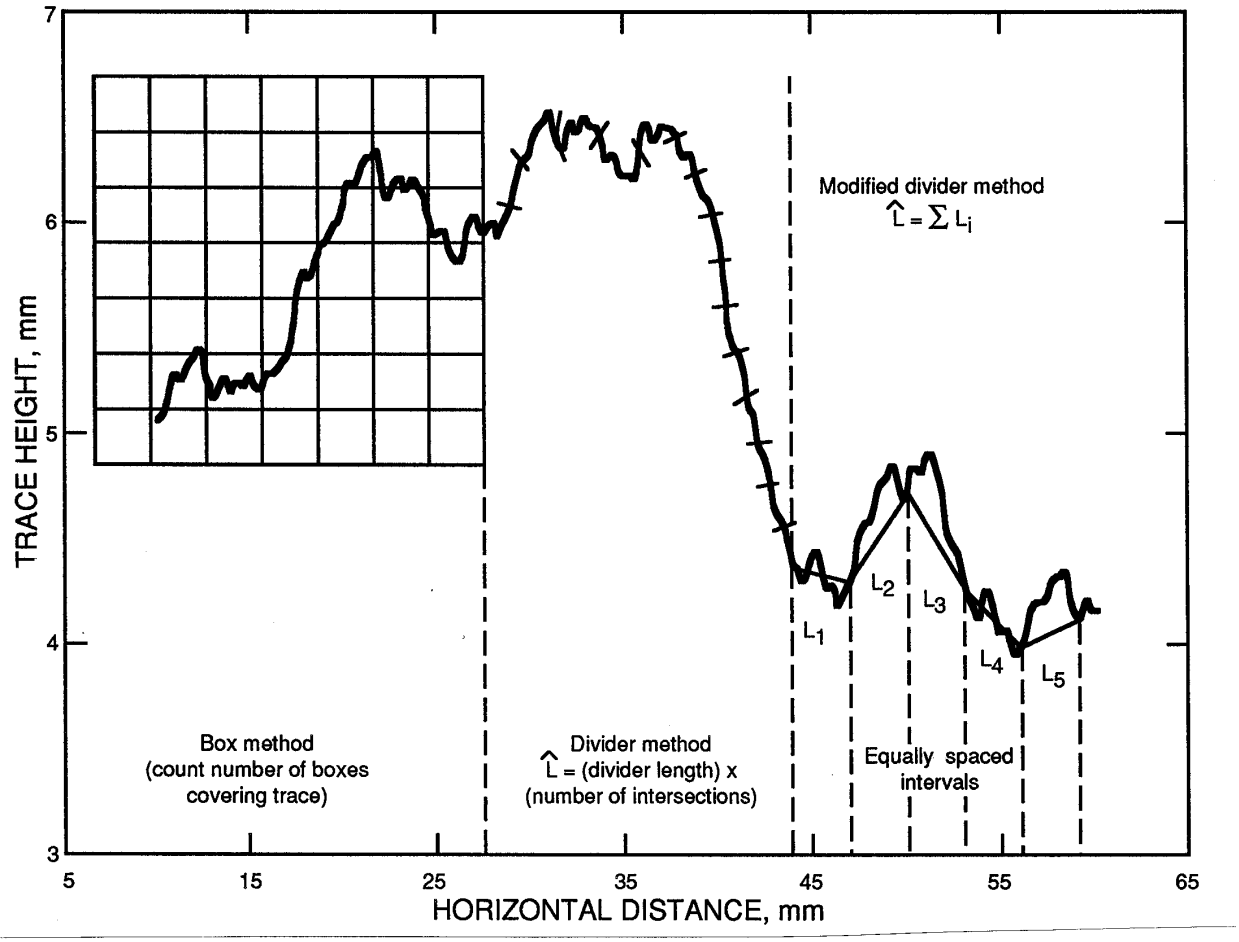

Figure 2.—Box and divider methods for estimating fractal dimensions. (L = estimated profile length.)

the entire profile is counted. Two versions of the box method were used in this study, one taken from Brown (*11*) and one from Feder (*20*). Brown's approach requires that the box grid be formed by taking an equal number of divisions in the x- and y-directions, which maintains an aspect ratio consistent with that of the profile, and then determining the relationship between the number of divisions and the number of boxes. In Feder's approach, the relationship between a box-size multiplier and the number of boxes required to cover the profile is determined. It was found that both methods provide similar estimates of D if the specified box sizes are comparable. For computational convenience, Brown's method was preferred, where D is estimated by

$$\log(N) = A + D \cdot \log(g),$$

where N = number of boxes required to cover the profile,

and g = number of box grid divisions in the x- and y-directions.

In this case, D = slope of the log-log plot.

In using the divider and box methods described above, appropriate adjustments were made to mitigate the crossover length problem associated with roughness profiles, as discussed by Brown (*12*). For the divider methods, the y-coordinate of the profiles was multiplied by 1,000. For

the box method, an equal number of box divisions were used in the x- and y-directions to ensure an aspect ratio equal to that of the profile. Analyses were also done with divider methods using no exaggeration of the y-coordinate values.

Spectral Method

The fractal dimension of a surface roughness profile can be related to the power spectral density S(F) of the profile, if one assumes a spectral density with power-law form, where $S(F) \propto F^{-b}$ and F = frequency in units of cycles per millimeter. In this case, D is related to slope b of the spectral density (*13*) according to b = 2D - 5.

Caution must be exercised when interpreting fractal results obtained from the spectrum, however, because assumptions of stationarity, ergodicity, and random phase may not be met by the profiles being studied (*25*).

The spectral density of each roughness profile was estimated using the fast Fourier transform method as discussed by Bendat and Piersol (*9*). This approach requires the investigator to select a tapering window and a spectral smoothing algorithm.

APPLICATIONS OF COMPUTER ALGORITHMS TO DATA

In applying the four computer algorithms—box, divider, modified divider, and spectral—it became apparent that there were difficulties specific to each method. For example, when using Brown's aspect ratio concept (*11*) with the box method, an equal number of divisions are made along both axes of the original profile data. The fractal dimension is computed from a derived log-log relationship, where the x-axis is the log of the aspect ratio and the y-axis is the log of the number of boxes intersected by the profile. The slope of a line fit to this log-log plot is the fractal dimension value.

Inherent in this method is the hypothesis that a straight line is a good model for the log-log data (fig. 3). However, there are at least three plausible but very different answers for the fractal dimension, varying from 0.94 to 1.19, depending on which set of box sizes the user chooses.

When using both divider methods, the procedures are similar. The x-axis of the derived plot equals the log of the divider span; the y-axis is the log of the corresponding profile length; and the fractal dimension equals 1 - slope of the log-log plot. In both methods, the log-log plots are similar in ambiguity, and the fractal dimensions can vary significantly, depending on the set of divider spans specified for measuring the profiles.

Even if a roughness profile reasonably meets stationarity and random-phase assumptions, fractal dimensions estimated using the spectral method can depend significantly on user specifications for obtaining the spectral density of the profile. The two most apparent specifications are the tapering window used to mitigate leakage and the algorithm used to smooth the spectral estimates

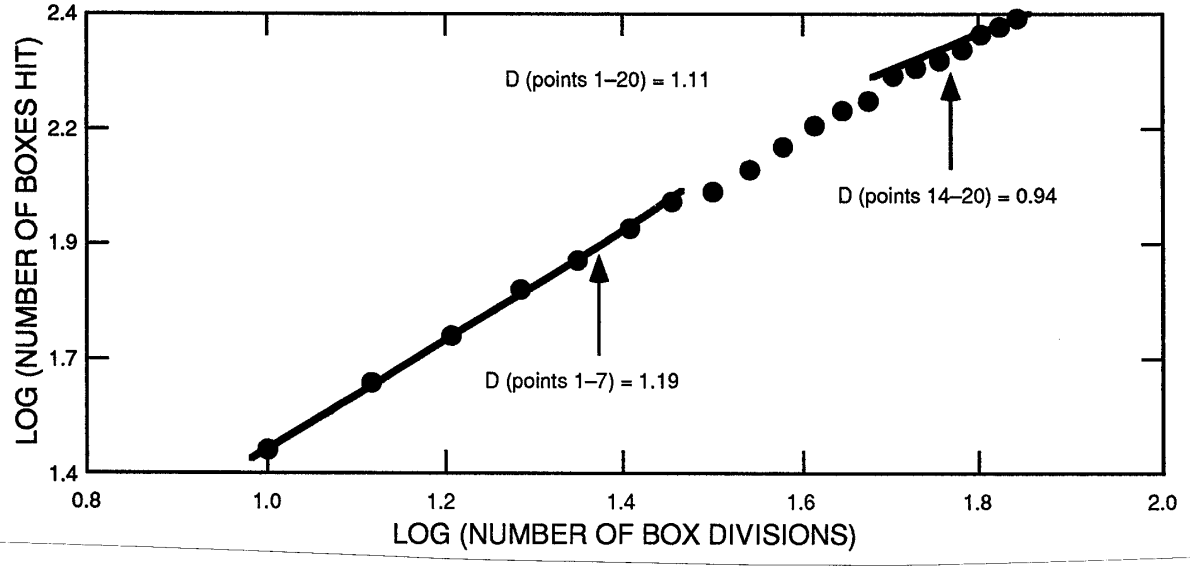

Figure 3.—Log-log determination of fractal dimension, box method.

(*9*, *41*). Repeated investigations of computed spectra of the roughness profiles showed that aliasing was not a problem (i.e., the spectra fell off to near zero at frequencies of 3 to 4 c/mm, much less than the Nyquist frequency of about 9.7 c/mm). Thus, leakage was the major concern, and even if a standard Tukey-Hanning smoothing function was consistently used for the spectral estimates and only the type of tapering window was varied,[6] quite different fractal dimensions were obtained for a given roughness profile (fig. 4).

Microcomputer programs written to calculate D were based on the four methods. Three of these programs were cross-checked with programs written by other computer programmers. The answers generated by the comparisons were quite consistent, giving the authors assurance that the computer programs were not sources of error.

Experience in analyzing the 60 roughness profiles indicated that the divider method was the most difficult of the four methods to use consistently and still obtain reasonable estimates of fractal dimension. The divider method does not provide unique results, and estimates of D may vary by 10 to 20 pct for a given profile. However, some of this ambiguity can be mitigated by selecting those divider spans that require 30 to 200 intersections to cover the profiles, which have approximately 1,000 digitized points. In addition, there are several ways to deal with remainders left when the divider increments approach the end of the profile trace (*3*). It is recommended that the

[6]The following tapering windows were used: cosine-bell with 2, 5, and 10 pct and full applications; Parzen; and Welch. Estimated fractal dimensions varied from 1.34 (for 2 pct cosine-bell window) to 1.49 (for Welch window).

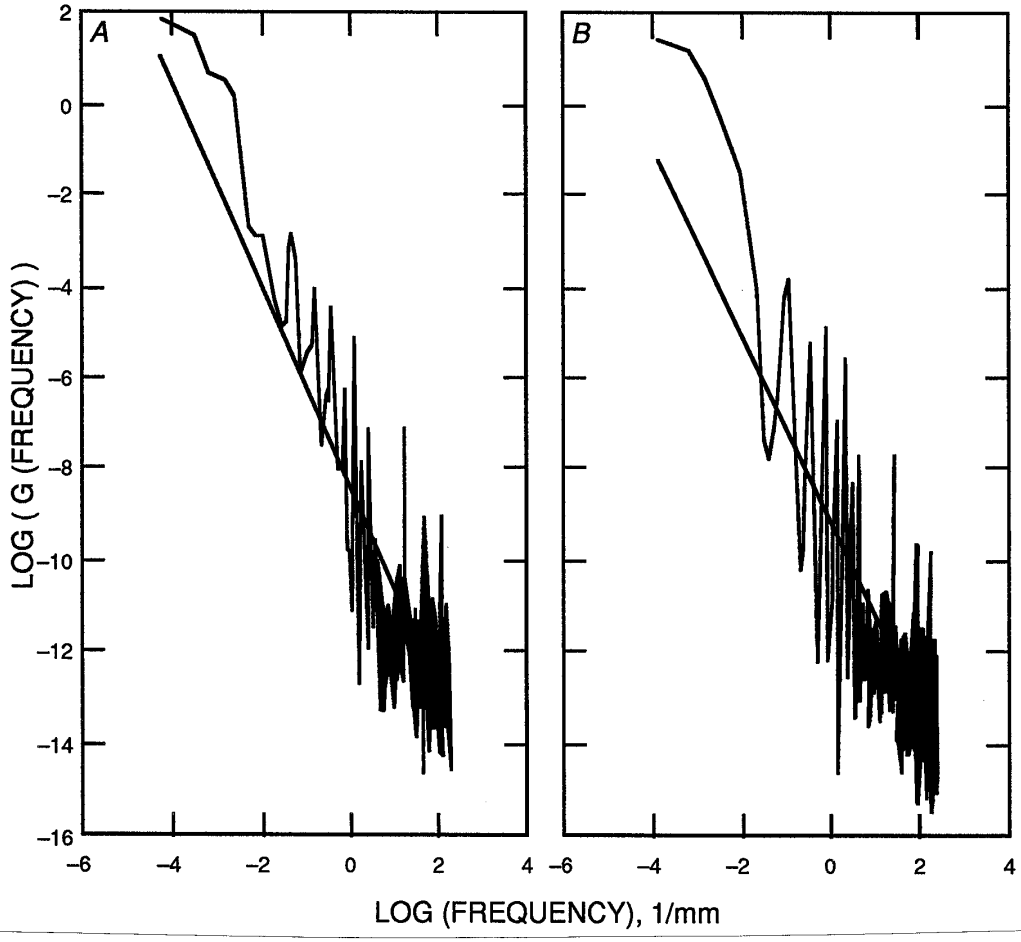

Figure 4.—Examples of log-log spectral plots showing the sensitivity of calculated fractal dimension to tapering. *A*, 2 pct cosine-bell window; *B*, Welch window.

partial divider length required to reach the end of the profile be divided by the selected divider span and then added to the number of divider spans already accumulated (e.g., the final number of spans might be 80.25, where the remainder is one-fourth of the selected divider span).

To alleviate the remainder problem when using the modified divider method, it is suggested that only those x-increments that terminate at an x-coordinate within $0.005L_h$ of the end of the profile (L_h = horizontal length of profile) be used. In addition to using this criterion, when computing fractal dimensions for the 60 profiles, investigators made sure that the largest x-increments were those that required at least 20 repetitions to cover the profile being studied.

When the box method was evaluated, the greatest success came when box sizes were used that allowed 20 to 120 boxes to cover the profile. Again, this criterion was based on profiles having about 1,000 digitized points. With the spectral method, a 2 or 5 pct cosine-bell tapering window provided the most consistent results.

Thus, using the above guidelines for the various methods, the fractal dimensions of all 60 profiles were computed and compared.

ANALYSIS OF ROUGHNESS MEASURES

Besides fractal dimension, there are several other measures that can be used to quantify roughness along rock fractures. The two we investigated were the Z_2 measure proposed by Myers (*38*) and the standard deviation of heights.

Calculation of the Z_2 measure for profiles is facilitated by using a slightly modified version of the original Myers definition (*38*), as proposed by Tse and Cruden (*44*):

$$Z_2 = \sqrt{\frac{1}{M(\Delta x)^2} \sum_{i=1}^{N-1} (y_{i+1} - y_i)^2},$$

where N = number of digitized values,

M = number of intervals on x-axis = $N - 1$,

and Δx = width of digitized x-increment.

The Z_2 measure is related strongly to the variance of slopes along the profile. To eliminate the effect of trends in the roughness profiles (i.e., regional slope) on the calculated standard deviation of heights, a linear trend was removed from each profile before calculating its standard deviation. It is realized that this detrended standard deviation does not serve as an adequate measure of roughness in itself, but it was included as a standard reference value for comparing with other roughness measures.

Comparison of Adjacent Profiles

To investigate surface roughness variability, for each set of 10 parallel profiles, the autocorrelations of the Z_2 measure and of the fractal dimension derived from the modified divider method were calculated. One of the appealing aspects of fractal analysis is that the fractal dimension of a topographic surface can be obtained by adding 1.0 to the fractal dimension of a single profile from that surface (*32*). However, the question arises as to which profile to use when rock fractures are being studied; that is, are such profiles relatively similar along a fracture surface? The autocorrelation results shown in table 1 (an autocorrelation of 1.0 implies perfect correlation) indicate that roughness profiles can be quite different, even when taken parallel to each other. In this case, the parallel profiles in each set were spaced 50 mm apart.

Table 1.—Autocorrelations of Z_2 and fractal dimension D for adjacent profiles on fracture surfaces

Measure	Basalt x	Basalt y	Gneiss x	Gneiss y	Quartzite x	Quartzite y
Z_2 ...	0.351	-0.030	-0.084	0.349	-0.072	0.228
D	.566	-.299	-.056	.101	.056	-.135

Correlation of Roughness Measures

Linear correlation coefficients were computed for the six roughness measures for each of the six profile series. Four of the measures were fractal dimensions calculated by the different methods: D_b by box method, D_d by divider method, D_m by modified divider method, and D_s by spectral method. Typical results are displayed in table 2. The negative correlation values indicate that the nonfractal roughness measures were inversely related to D estimates. Values of D computed by the two divider methods were the most strongly correlated, followed by those computed by the spectral method. The nonfractal measures of roughness were correlated strongly.

Surprisingly, the D_s-standard deviation and the D_s-Z_2 correlations were negative. This finding contradicts theoretical relationships where variance of heights is the 0th moment of the spectrum and variance of slopes is the 2d moment of the spectrum (*13*). Because computer-generated synthetic profiles produced correlations that agreed with the stated theory, the above contradictions may be caused by the scale dependence of Z_2 and standard deviation and/or by the failure of the roughness profiles to be modeled adequately by random processes.

Evaluation of Roughness Measures Using Visual Assessments of Roughness

Because the two different sets of roughness measures appeared to be so different when applied to these rock fractures, the measures were evaluated using visual observations of the roughness profiles. The 10 profiles for the gneiss x-direction series are shown in figure 5.

To evaluate the performance of each roughness measure, four investigators were asked to independently rank the roughness of profiles in each series on a scale of 1 to 10 (1 was smoothest and 10 was roughest) according to visual observations. These roughness rankings were tabulated with rankings obtained using the six roughness measures, plus another parameter, A_m, which is equal to the y-intercept of the log-log plot of the modified divider algorithm. These numbers were used to compute values of Kendall's nonparametric rank correlation coefficient (*42*). Typical rank correlation results are summarized in table 2 and illustrate the general conclusion that calculated fractal dimensions can be, and often are, negatively correlated with visual rankings of roughness profiles.

Table 2.—Roughness measures, gneiss x-direction series

	D_b	D_d	D_m	D_s	A_m	Z_2	Standard deviation	Visual rank
CORRELATION MATRIX								
D_b	1.000							
D_d	.551	1.000						
D_m	.580	.857	1.000					
D_s	.522	.793	.746	1.000				
Z_2	-.288	-.848	-.677	-.828		1.000		
Standard deviation	-.719	-.859	-.788	-.832		.792	1.000	
SUMMARY OF PROFILES								
Profile:								
A	1.099	1.161	1.129	1.258	3.569	0.171	0.201	6
B	1.158	1.192	1.123	1.246	3.546	.169	.199	5
C	1.118	1.193	1.157	1.202	3.592	.186	.268	7
D	1.159	1.094	1.103	1.191	3.813	.282	.385	9
E	1.143	1.261	1.199	1.383	3.377	.131	.118	1
F	1.122	1.155	1.128	1.309	3.495	.149	.202	2
G	1.136	1.182	1.200	1.263	3.573	.179	.238	4
H	1.146	1.183	1.147	1.274	3.536	.161	.271	3
I	1.076	1.105	1.103	1.225	3.731	.213	.479	8
J	1.041	1.084	1.058	1.124	3.816	.245	.618	10
Rank correlation coefficients versus visual rank	-.289	-.511	-.556	-.911	.911	-.867	.600	

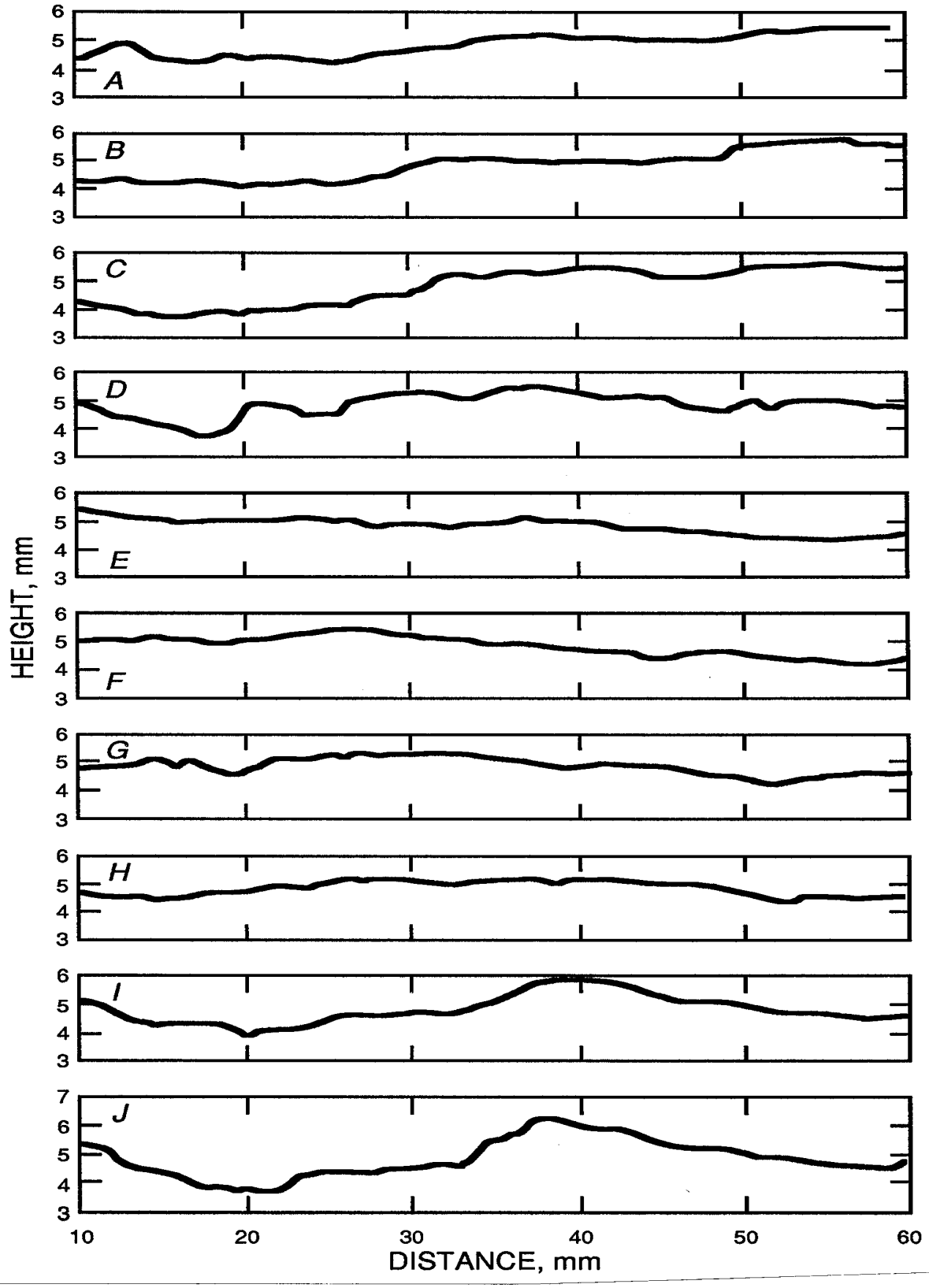

Figure 5.—Ten gneiss profiles (traces A-J) oriented in x-direction.

ADDITIONAL TOPICS ON FRACTALS AS A MEASURE OF ROCK FRACTURE ROUGHNESS

INTRODUCTION

The work on shear strength used the gneiss specimen in the x-direction only (*34*). The work described in the following sections applies the fractal geometry approach to the gneiss y-direction and the quartzite and basalt x- and y-directions also. There were several topics investigated, including the effects of using enlarged photographs, the aspect ratio concept (*11*), the separate data set supplied by the Centre de Technologie Noranda, the use of profiles versus three-dimensional modeling, and the fractal controversy.

EFFECT OF ENLARGED PHOTOGRAPHY

One possible source of error in the photogrammetric studies was the physical size of the photographs being read and digitized. Since the scanning dot size (0.05 mm) was quite large relative to the interval between data points, it was suggested that enlarging the photographs of the samples might provide more representative results. Thus, the photographs were enlarged 2.44 times. Care was taken to align traces exactly. For this work, gneiss x-direction readings were used. So that comparisons could be made, it was necessary to truncate the original readings to a smaller set of information (80 pct of original trace length); thus correlation values differed from those discussed in the section "Analysis of Roughness Measures" (compare table 3 with table 4). As before, 10 profile traces were analyzed to generate the set of derived fractal dimensions and Z_2 measures. The y-coordinates were scaled two ways: with Brown's aspect ratio (*11*) and with a scale factor equaling 1. The latter case is denoted as the original data space analysis throughout the rest of this RI. "Regular" refers to the standard-sized photographs while "enlarged" refers to the enlarged photographs.

Aspect Ratio Analysis

As explained earlier, linear correlation coefficients were computed for the four roughness measures and for the Z_2 measure (table 4). It can be seen that the same basic trends hold: that the fractal measures were not strongly correlated with each other and were, with one exception, negatively correlated with the Z_2 measure. The fractal measures were slightly better self-correlated for the data set from the enlarged photographs than for the data set from the regular photographs, while the set of enlarged profile traces generated more robust fractal dimension values (i.e., higher mean value and greater variation). This was true when using the box, divider, and modified divider methods. However, the spectral method did not display this robust quality; here, the fractal dimension values from the regular photographs had a higher mean and greater variation.

Table 3.—Correlation matrix for roughness measures and shape parameters for nonlinear, shear-strength envelope

	A	B	D	I	Z_2
A	1.000				
B	-.489	1.000			
D	.637	-.578	1.000		
I	-.467	.785	-.267	1.000	
Z_2	-.775	.678	-.704	.534	1.000

Table 4.—Correlation matrix for roughness measures using aspect ratio method, gneiss x-direction series

	D_b	D_d	D_m	D_s	Z_2
REGULAR PHOTOGRAPHS					
D_b	1.000				
D_d	.273	1.000			
D_m	.471	.827	1.000		
D_s	.237	.846	.588	1.000	
Z_2	.051	-.882	-.608	-.822	1.000
ENLARGED PHOTOGRAPHS					
D_b	1.000				
D_d	.665	1.000			
D_m	.695	.817	1.000		
D_s	.672	.822	.590	1.000	
Z_2	-.522	-.742	-.390	-.919	1.000

Another comparison of interest was the correlation between the regular and enlarged results for the 10 profile traces analyzed by the five measures of roughness. The results are shown in table 5.

Table 5.—Roughness measure correlations between regular and enlarged data set

Method	*Correlation coefficient*
D_b	0.584
D_d	.980
D_m	.777
D_s	.935
Z_2	.976

If one were to hypothesize similarities between the regular and enlarged photographs, high correlation values

would be anticipated, and in fact, in three of the five cases, high correlations were obtained.

Rank correlation coefficients (*42*) were computed comparing the visual assessments with the roughness measures. Results are summarized in table 6.

Table 6.—Rank correlation coefficients of roughness measures versus visual rank using aspect ratio method, gneiss x-direction series, y-coordinate

	D_s	D_b	D_d	D_m	Z_2
Regular . . .	-0.951	-0.042	-0.733	-0.697	0.867
Enlarged . .	.335	-.564	-.685	-.418	.822

Both photographic methods generated similar results; only the Z_2 measure correlated positively with the visual rankings, while the four fractal methods correlated negatively (in seven of the eight cases) with the visual assessments.

Original Data Space Analysis

Only two measures, D_m and Z_2, were used. For the regular photographs, the correlation between D_m and Z_2 was 0.945; for the enlarged photographs, the correlation between D_m and Z_2 was 0.954. This is quite significant in that the fractal measure was strongly positively correlated with the Z_2 measure in contrast with results obtained by comparing aspect ratios. The correlation for D_m (regular versus enlarged data set) was 0.969, which was also a better answer than the 0.777 obtained for the aspect ratio. Correlations between D_m and the visual rankings were 0.764 (regular data) and 0.733 (enlarged data). Two major conclusions were reached:

1. The regular and enlarged data sets behaved similarly when using a scale factor of 1, and
2. A scale factor of 1 promoted better agreement between D_m and Z_2 than did previous analyses of the gneiss x-direction data. This point will be expanded upon in the section "Gneiss y-Direction Analysis."

Thus, it was felt that the enlarged photographs generated results similar to those obtained from the regular-sized photographs, and that using enlargements will not produce more satisfying results.

FRACTAL DIMENSION AND ASPECT RATIO CONCEPT

A perplexing problem facing users of the fractal dimension as a measure of profile roughness is the small magnitudes of the generated fractal dimension values. Using the divider method, the authors generated a fractal dimension of 1.3 for the coast of Britain and 1.52 for the coast of Norway (*20*). Both coastlines represent highly perturbated profiles, yet these fractal dimensions are rather modest. In studying profiles taken from rock surfaces adjacent to Libby Dam, MT, Carr and Warner (*15*) attained fractal dimension values of 1.0031, 1.0032, 1.0220, etc. Applying the divider technique to nonscaled profiles for the rock surfaces studied here generated fractal dimensions similar to those found by Carr and Warner. Furthermore, when the divider technique was applied to fractal-generated profiles of known dimensions (e.g., 1.2, 1.3, 1.5), the fractal dimensions gave results much less than these known dimensions. The divider method is not unique with regard to this shortcoming; the box-counting method presents similar problems.

Two authors, Wong (*46*) and Brown (*11*), have recognized and dealt with this problem, which is referred to as the crossover length problem and is best defined in terms of the basic divider method. There exists a critical divider length (crossover length) such that if the chosen divider radii are larger than the crossover length, the fractal dimension will be very close to unity. Brown suggests solutions for the crossover problem as follows:

1. For the divider method, multiply the z-coordinate (only) by increasingly large values, e.g., 10, 100, 1,000,... If one does this, the fractal dimension will indeed asymptote to a value that is not necessarily near unity, but this value should be more representative of the true fractal dimension.[7] This transformation of the z-coordinate only may result in an extremely exaggerated portrayal of the original trace. Effectively, all variability has been transferred to the z-variable alone.
2. For the box-counting method, choose an equal number of intervals (for division into box size) along both the x- and z-axes. Brown (*11*) develops the mathematics for this option.[8] Using Brown's aspect ratio concept provides excellent verification for generated profiles of known fractal dimension, thus giving credence to the consistency of this approach.

Several scientists question transforming a profile so drastically in order to attain a consistent fractal dimension. The authors of this RI used the aspect ratio concept exclusively for two symposium papers (*36-37*). In these papers, the authors endeavored to look at the data with and without using aspect ratio algorithms. At this juncture, it seems unclear as to whether one should commit unequivocally to either school of thought on the subject of aspect ratio.

[7]Brown's approach (*11*) circumvents one's actually finding the critical crossover length, which is certainly a useful technique.

[8]This approach provides a very pragmatic artifice for users of the box method because determination of the box's physical dimensions is critical to generation of a "correct" fractal dimension. Feder (*20*, pp. 186-188) demonstrates varying the fractal dimension from 1.03 to 1.51 based on the dimensions of the boxes chosen.

EFFECTS OF PARAMETER INPUT ON FRACTAL DIMENSION

The selection of parameter values has a marked effect on the calculated fractal dimension. When using fractal algorithms, the user must be aware that one cannot just operate on automatic pilot and generate significant answers. Two illustrations are provided, one relative to the box algorithm, the other to the modified divider algorithm.

Parameter Effects—Box Algorithm

An artificially generated profile trace with 1,200 data points and a known fractal dimension of 1.3 was used as the example (fig. 6). The dependent variable had a mean of 7.212 and a standard deviation of 1.295. The generation routine was a spectral analysis synthesis method proposed by Saupe (5, pp. 93-94). The advantage of this generated profile was that the property of self-affinity was guaranteed. Visually, one would feel comfortable in assuming that the trace was of a fractal nature.

The set of aspect ratio values that proved most successful relative to the bulk of the experimental data was used. The computer output is listed in table 7.

The fractal dimension 1.166 obtained earlier was certainly unsatisfactory relative to the expected value of 1.3. However, if the user were to choose aspect ratio input values running consecutively from 2 to 20, the generated fractal dimension would be 1.335, with a correlation coefficient value of 0.9965. This seems more in line with

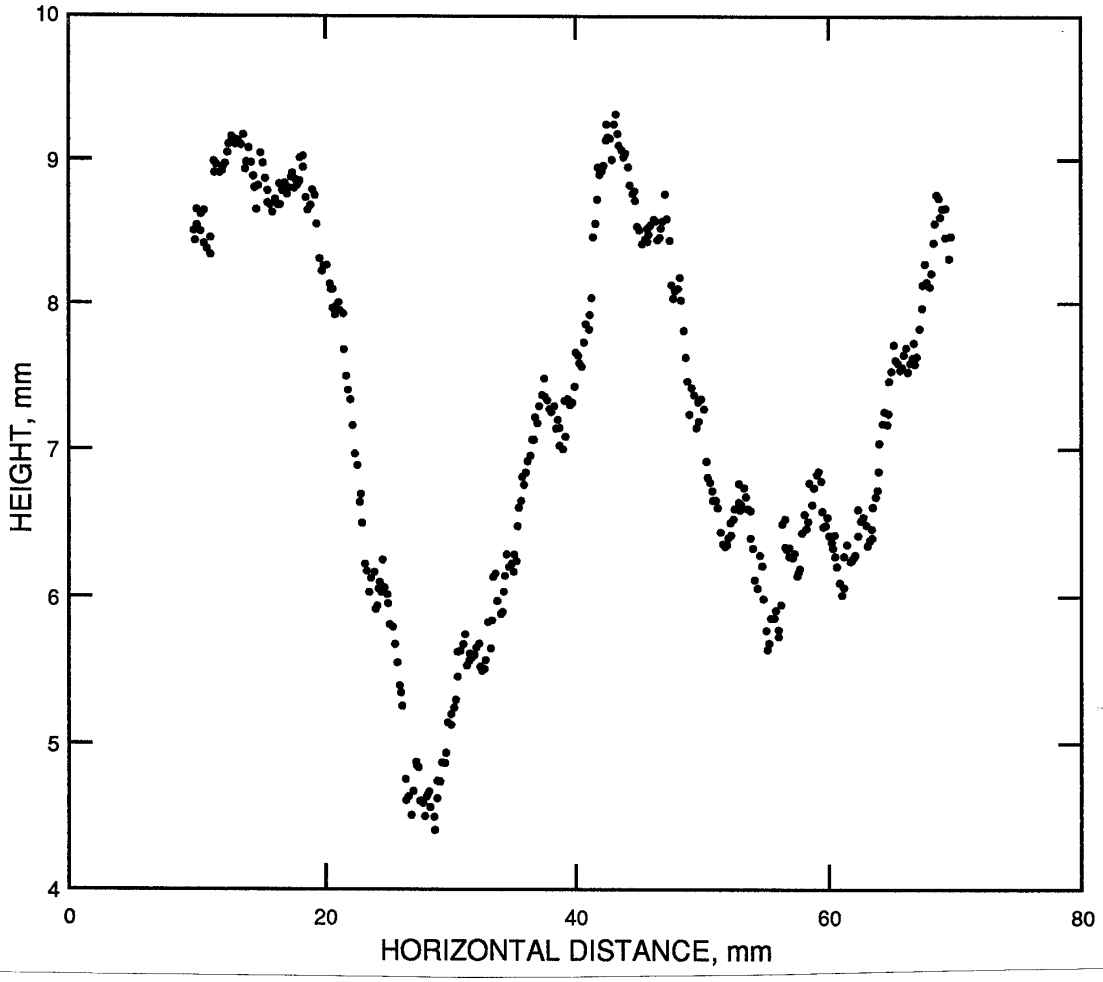

Figure 6.—Generated fractal profile with fractal dimension of 1.3.

expectations, but the boxes for the low aspect values (2 and 3) were completely filled! Thus, the curves were loaded if this selection was made (table 7).

Table 7.—Computation of fractal dimension using box method (expected value = 1.3)

	Aspect ratio	Number of boxes
Input values consistent with prior analysis[1] . .	10	45
	15	73
	20	103
	22	114
	25	132
	27	145
	30	166
	35	198
	40	221
	45	264
Input values varied[2] . .	2	4
	3	9
	4	13
	5	18
	6	22
	18	89
	19	92
	20	103
First point removed[3] . .	3	9
	4	13
	5	18
	6	22
	18	89
	19	92
	20	103

[1]Fractal dimension = 1.166; correlation coefficient = 0.9997.
[2]Fractal dimension = 1.335; correlation coefficient = 0.9965.
[3]Fractal dimension = 1.269; correlation coefficient = 0.9987.

The point (2,4) log values of (0.3010, 0.6021) were exercising undue influence on the slope of the fitted line and were a candidate for dismissal as an outlier. This decision could be justified on other grounds because 100 pct of the boxes were filled when only two subdivisions were made on the coordinate axes. If the point (log 2, log 4) were left out, but (log 3, log 9), which represents another set of totally filled boxes, were allowed to remain, then the point (log 3, log 9) lies on a line consistent with the remaining set of values (figure 7 and table 7).

By removing one data point, the fractal dimension was changed from 1.335 to 1.269. This parameter variation could be continued through many possible combinations of aspect values and would generate changes in the fractal dimension. This exercise illustrates how the selection of input values would change the fractal dimension, in this instance, from 1.666 to 1.335. (Again, recall that the expected fractal dimension is 1.3.) These changes were not a consequence of using the aspect ratio method. Feder (*20*, pp. 186) changes the rectangular dimensions of the covering of boxes, and in so doing, varies the fractal dimension from 1.03 to 1.51. Thus, the user's selection of input values can directly affect the resulting fractal dimension, certainly not a desirable situation when one is seeking invariance or stability of answers from a procedure.

Modified Divider Algorithm and Scaling Factor Variations

Earlier, the modified divider technique was used in conjunction with a z-coordinate (i.e., trace height) scaling factor to alleviate the crossover length problem. A set of profile traces with given fractal dimension values of 1.05, 1.2, 1.3, 1.4, and 1.5 and a sample size of 1,200 was generated by spectral synthesis (*5*). Table 8 shows the progression of the fractal dimension values as a function of the scaling factor.

Table 8.—Effect of scaling factor on fractal dimension computations using modified divider algorithm

Generated fractal dimension	Z-coordinate scale factor				
	1	5	10	100	1,000
1.05	1.012	1.080	1.110	1.132	1.132
1.20	1.038	1.174	1.213	1.240	1.241
1.30	1.079	1.261	1.301	1.327	1.327
1.40	1.147	1.362	1.398	1.418	1.418
1.50	1.246	1.467	1.497	1.513	1.513

Several points become apparent. First, a scaling factor of 1.0 underestimated the expected (generated) fractal dimension values in all cases. Second, the expected fractal dimension of 1.05 was poorly estimated throughout. Third, a scaling factor of about 10 seemed to be a best choice for this set of data in that the expected fractal dimensions were reasonably close to the derived values. Fourth, the fractal dimension values asymptote to a constant as the scale factor increased.

As before, a potential problem arises in that user input of best scale factor is implied. With experimental data, there are no guidelines as to what the best choices might be, leaving the user with difficult decisions as to what scale factor to choose. In previous work, the asymptotic approach was chosen, using a scale factor of 1,000.

GNEISS y-DIRECTION ANALYSIS

For the same sample used in the section "Analysis of Roughness Measures," 10 profiles oriented along the y-axis were also digitized using photogrammetry. Four fractal dimension algorithms and two statistical algorithms were applied to these profiles. Descriptive statistics were computed relative to these derived measures of the 10 traces,

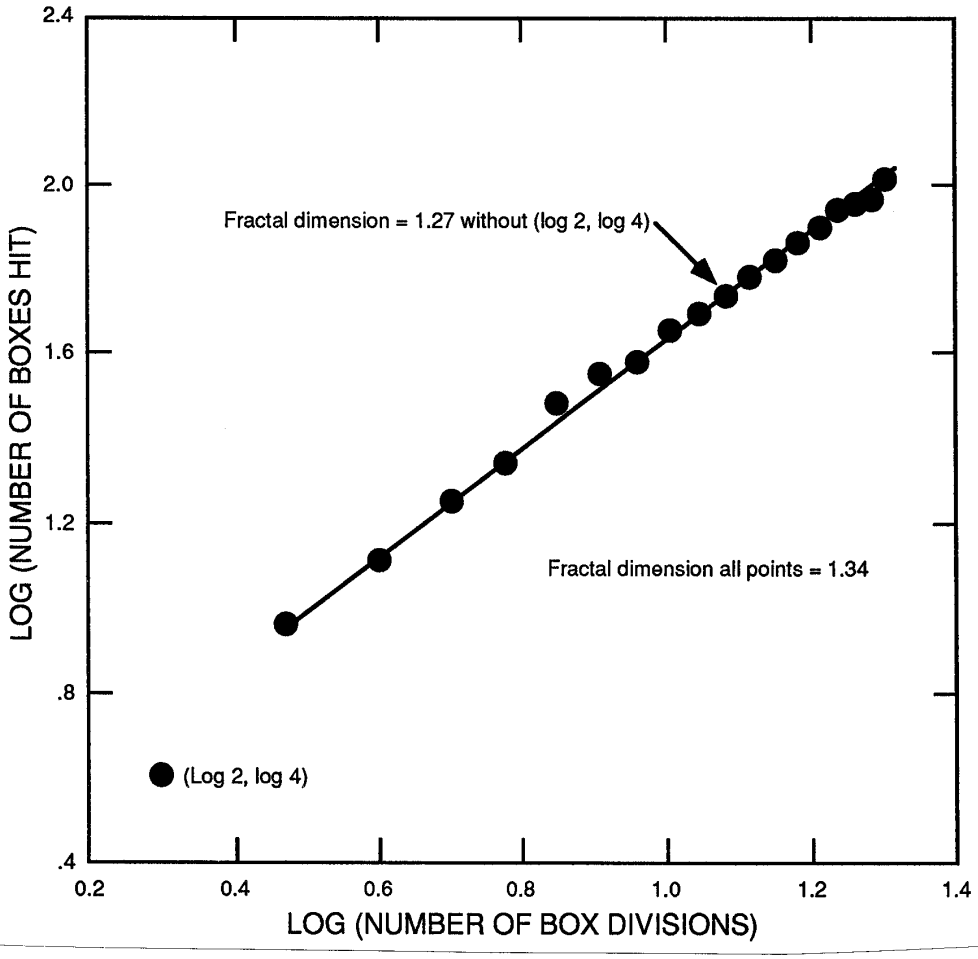

Figure 7.—Effect of one data point on calculated fractal dimension.

giving values for mean, median, standard deviation, standard error of the mean, etc. Correlations were established between the six algorithms being considered (table 9).

Table 9.—Correlation matrix for roughness measures using aspect ratio method, gneiss y-direction series

	D_b	D_d	D_m	D_s	Z_2	Standard deviation
D_b	1.000					
D_d	.513	1.000				
D_m	.587	.924	1.000			
D_s	.433	-.054	-.007	1.000		
Z_2	.561	.167	.412	.432	1.000	
Standard deviation	-.572	-.793	-.813	-.139	-.323	1.000

Table 9 is to be compared with table 2. In table 2, there is a nice dichotomy between the four fractal measures—D_b, D_d, D_m, and D_s—and the statistical measures—Z_2 and standard deviation. The fractal measures are positively correlated with each other and negatively correlated to the statistical measures. The two statistical measures are positively correlated. In table 9, three of the fractal measures—D_b, D_d, and D_m—are positively correlated with each other, but D_s does not conform to family behavior as before. Furthermore, Z_2 is now positively correlated with the fractal measures; only the standard deviation stands alone.

Four investigators were again asked to rank the roughness measure of the 10 gneiss y-profiles subjectively (fig. 8). Their visual rankings were then compared with

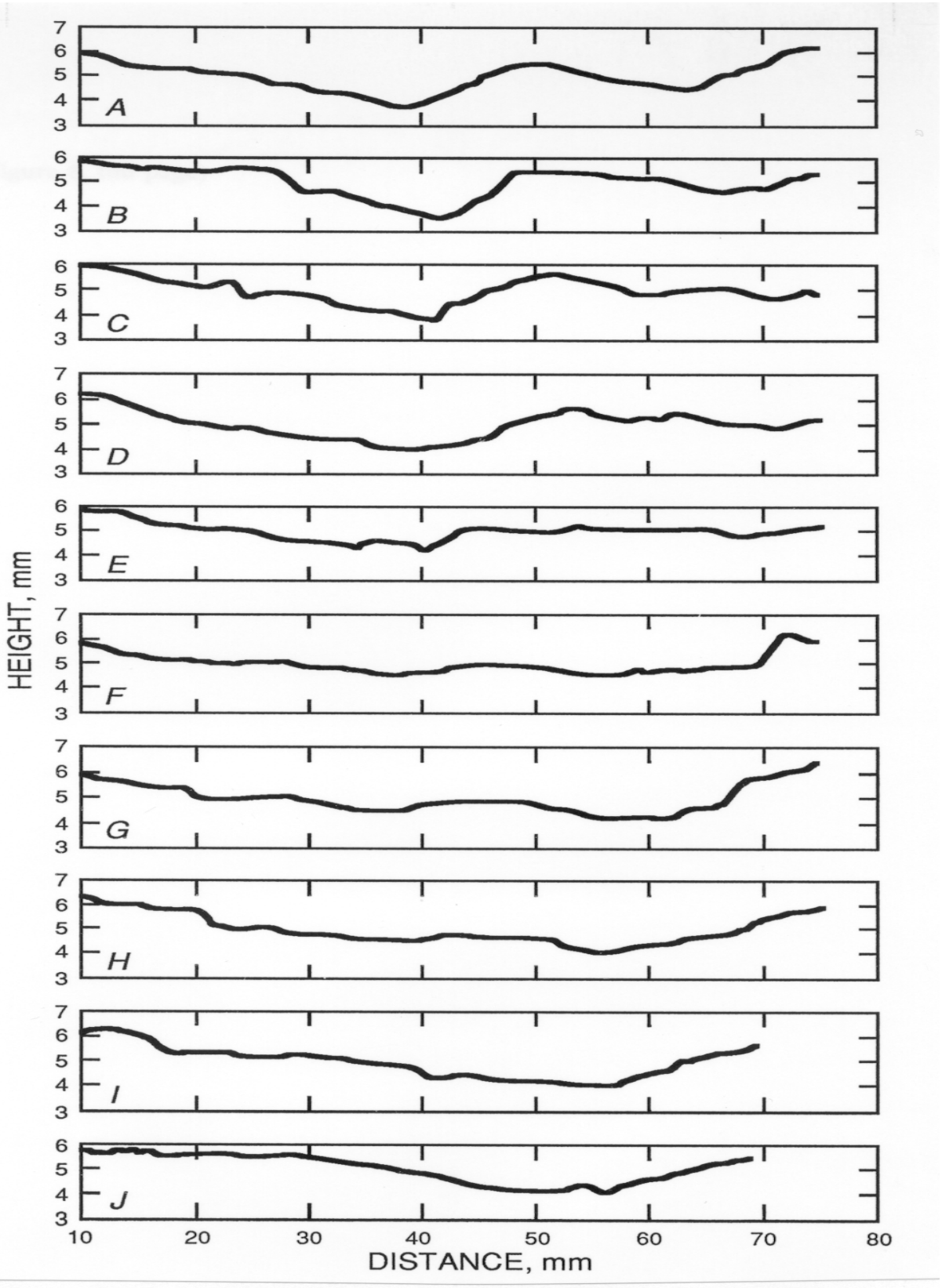

Figure 8.—Ten gneiss profiles (traces A-J) oriented in y-direction.

the ranking obtained by the six roughness measures, after which Kendall's nonparametric rank correlation test (*42*) was applied. Results are tabulated in table 10.

Table 10.—Rank correlation coefficients of roughness measures versus visual rank, gneiss x- and y-direction series

	D_b	D_d	D_m	D_s	A_m	Z_2	Standard deviation
x-direction	-0.289	-0.511	-0.556	-0.911	0.911	-0.867	0.600
y-direction	-.244	-.556	-.368	.135	.822	.252	.378

These results were not as encouraging as those shown for the x-direction profiles, and only A_m was highly correlated with the visual assessment.

Another way to compare the answers in the x- and y-directions is to consider the 10 x-traces and the 10 y-traces as populations and to use a statistical t-test to test for equality of means. Table 11 summarizes the results and demonstrates the anisotropic nature of the gneiss rock sample.

Table 11.—Comparison of six roughness measures using aspect ratio method on gneiss specimen, x- versus y-direction

Method	*t-value*[1]
D_b	1.86
D_d	2.80
D_m	3.63
D_s	2.03
Z_2	.48
Standard deviation	3.31

[1]Degree of freedom are greater than 11 in all cases.

Similar analyses were applied to the x- and y-directions of a basalt sample and a quartzite sample. The anisotropy shown in the gneiss sample was also apparent in both the basalt and the quartzite samples.

In summary, the y-direction analysis of the gneiss sample did not generate results that were consistent with those obtained for the x-direction analysis. Furthermore, the y-direction results would not lead to the same approach to shear strength modeling as used in the section "Shear Strength Estimation." However, the data for the x- and y-directions for the gneiss, basalt, and quartzite samples were fit reasonably well by the model developed in that section. With regard to the most important conclusion of this RI—the ambiguities of the fractal dimension measures and their contrast with the statistic measures—work with the gneiss y-profiles and the basalt and quartzite x- and y-profiles further substantiated the ambiguity premise.

ORIGINAL DATA SPACE ANALYSIS, GNEISS x- AND y-DIRECTIONS

Brown's aspect ratio method (*11*) was used in the algorithms for the box, regular divider, and modified divider computations. As stated earlier, not all researchers are in favor of the aspect ratio technique. In this work, the z-coordinates (trace heights) of the profile traces were multiplied by 1,000 in computing the fractal dimensions for the divider and modified divider methods. The aspect ratio artifice was used in determining the number of divisions of both axes when applying the box-counting technique. The work that follows does not apply the scaling factor of 1,000 to the divider methods. The remaining fractal dimension algorithms (for D_b and D_s) and statistical algorithms (Z_2 and standard deviation) were computed as before. The goal was to find out whether better results were obtained using original data space information than were obtained using the scaling factor. The ensuing correlation matrices are shown in table 12.

Table 12.—Correlation matrix for roughness measures using original data space input, gneiss x- and y-direction series

	D_b	D_d	D_m	D_s	Z_2	Standard deviation
GNEISS x-DIRECTION SERIES						
D_b	1.000					
D_d	.034	1.000				
D_m	-.050	.966	1.000			
D_s	.522	-.659	-.720	1.000		
Z_2	-.288	.933	.925	-.828	1.000	
Standard deviation	-.719	.554	.534	-.832	.792	1.000
GNEISS y-DIRECTION SERIES						
D_b	1.000					
D_d	.071	1.000				
D_m	.397	.450	1.000			
D_s	.443	-.100	.270	1.000		
Z_2	.561	.367	.860	.432	1.000	
Standard deviation	-.572	-.056	-.551	-.139	-.323	1.000

The results in table 12 are to be compared with those in tables 1 and 8. There is no marked improvement in the correlations among the four fractal dimension algorithms, although in table 1, D_d and D_m are highly correlated (r = 0.966). But the data in table 12 show a low

correlation between D_d and D_m (r = 0.450). Z_2 correlates rather well with the fractal measures. The standard deviation does go its own way, being negatively correlated with all the fractal methods. Unfortunately, it is also negatively correlated with the other statistical measure, Z_2. Thus, when using the original space data, some correlations improve, while other correlations do not.

For the visual ranking of the gneiss profiles, the use of Kendall's rank correlation analysis (*42*) generated table 13.

Table 13.—Rank correlation coefficients using original scale data, roughness measures versus visual ranking, gneiss specimens

	D_d	D_m
x-direction	0.750	0.841
y-direction	.315	.225

Using the original scaled data gave much better results for the divider algorithms in the x-direction, but this comparison was rather inconclusive for algorithms in the y-direction. Augmenting this result with the preceding correlation matrices, the conclusion was that using the original scaled data represented no particular advantage over using the aspect ratio approach. In particular, the ambiguities between the fractal measures remained an important problem.

FRACTAL ALGORITHMS APPLIED TO NORANDA DATA SET

A reasonable question that must be addressed is: Are the fractal algorithm anomalies particular to the Bureau's Spokane Research Center (SRC) photogrammetric data set? To provide a partial answer, SRC researchers were fortunate to obtain a set of rock profile data collected by Noranda engineers. Noranda investigators hoped that a fractal dimension analysis would provide additional scientific insights, while SRC researchers appreciated the opportunity to verify fractal work using an independent set of profile information.

Profile traces were collected with a mechanical profilometer from a variety of sites. Typical profile lengths (fig. 9) were 100 cm, with over 800 usable data points per trace. (Profile lengths were over 10 times those of the SRC data, although the number of data points per profile trace was very similar.) Nine profile traces were collected per joint surface; three traces were oriented in a horizontal direction, three traces at 45°, and three traces in a vertical direction. Eighteen parameters were measured on each profile, including asperity angle, high and low peak values, amplitude parameters, and the Z_2 measure. The Z_2 measure provided a means of verifying that the Noranda data were properly transmitted for use at SRC.

Three sets of joints were selected from the Noranda data file, and three fractal algorithms, D_b, D_d, and D_m, were derived from the nine profile traces contained on a single joint surface. The aspect ratio was not applied when computing D_d. A representative set of Noranda results is shown in table 14. Then, to verify that the results were not unique, two other joint sets were analyzed; the results are shown in table 15.

Table 14.—Fractal dimensions and Z_2 for Noranda joint set NS2J1

Profile	D_b	D_d	D_m	Z_2
H211	1.154	1.0048	1.330	0.238
H212	1.082	1.0050	1.268	.323
H213	1.099	1.0055	1.274	.318
V211	1.096	1.0067	1.139	.346
V212	1.136	1.0052	1.194	.241
V213	1.111	1.0023	1.166	.176
A211	1.122	1.0034	1.287	.202
A212	1.168	1.0034	1.312	.184
A213	1.099	1.0043	1.330	.311

Table 15.—Correlation matrix for roughness measures, Noranda joint sets

	D_b	D_d	D_m	Z_2
NORANDA JOINT SET NS2J1				
D_b	1.000			
D_d	-.335	1.000		
D_m	.415	-.223	1.000	
Z_2	-.713	.838	-.169	1.000
NORANDA JOINT SET NS1J1				
D_b	1.000			
D_d	.076	1.000		
D_m	-.255	.158	1.000	
Z_2	.027	-.993	-.197	1.000
NORANDA JOINT SET NS1J5				
D_b	1.000			
D_d	.386	1.000		
D_m	.552	.272	1.000	
Z_2	.201	.932	.284	1.000

The expectation of high correlations was tempered by the fact that the Noranda traces were not collected as uniformly as were the SRC data. Here, nine traces per joint surface are included, but the traces are oriented into three triplets going in three different directions. Nonetheless, the joint surface provided a basis of commonality,

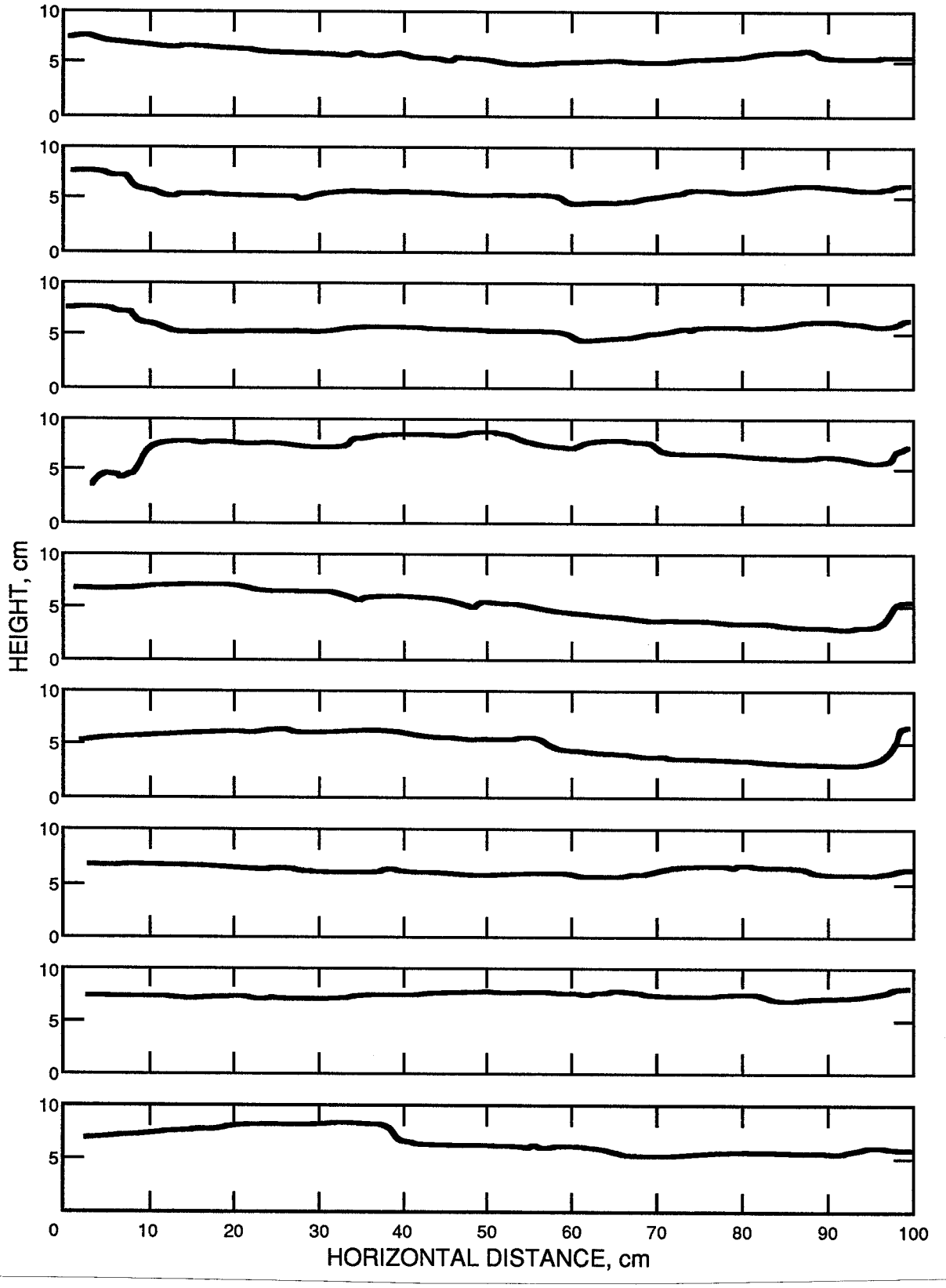

Figure 9.—Noranda profiles used in analysis. (Profiles were unidentified.)

and if the measures of roughness are uniform or consistent, it is to be expected that the resulting correlations should have reasonably high values as before.

The matrices displayed in table 15 seem to verify the SRC results. The intercorrelations between the fractal measures are again disappointing; in fact, the only high correlations in table 15 are between D_d and Z_2. Unfortunately, the correlation between D_d and Z_2 reverses algebraic sign for joint set NS1J5, thus negating positive speculation about the interrelationship of these two variables. Therefore, no new research directions or conclusions relative to fractal dimension measures evolved after considering the Noranda data.

FRACTAL CONTROVERSY

Much of the work discussed in this report was predicated on using the fractal dimension as a potential measure of the roughness of a rock joint surface. However, the field of fractal geometry evolved considerably during the period this research was being undertaken (1987-91). Many reputable scientists from many disciplines have written scholarly papers in which fractal geometry served as a major research tool (*16, 29, 45, 48*), particularly in the earth sciences. In 1985, Barton and Larsen published such a paper, "Fractal Geometry of Two-Dimensional Fracture Networks at Yucca Mountain, Southwestern Nevada" (*6*). The work of Brown (*11-13*) has been previously cited. The article by Aviles, Scholz, and Boatwright, "Fractal Analysis Applied to Characteristic Segments of the San Andreas Fault" (*3*), was published in 1987. Papers have been published relating the fractal dimension with earthquakes (*43*). In a recent paper by Coughlin and Kranz (*17*), the earthquake concept was successfully applied to relating the fractal dimension with rock-burst-associated seismicity. Feder (*20*) is an excellent practical source that contains many scientific applications.

Certainly the visual geometry generated by fractal techniques has captured the imagination of scientists, scholars, and others. As a generator of surfaces, fractal geometry has proven to be most successful. Beautiful two- and three-dimensional pictures have been produced by fractal generators, some of which were attractively displayed in a volume entitled "The Science of Fractal Images," by Barnsley, Devaney, Mandelbrot, Peitgen, Saupe, and Voss (*5*).

However, in spite of the positive applications of fractals, there is increasing criticism of the field of fractal geometry. Many practitioners have found that fractals are not necessarily the solution to their particular scientific problem. Fox's article (*22*) pointed out discrepancies between theory and empirical results with regard to using spectra to compute the fractal dimension. This is very significant, for most of the theoretical basis for the fractal dimension is derived from spectral considerations. Gilbert's article (*24*) also referred to untidy problems when using the spectral approach. In a very provocative set of articles and answering correspondence (*4, 30, 33*), two noteworthy opinions were put forth. Kranz (*30*) criticized the field of fractal geometry, stating that "Fractal geometry has not solved any problems. It is not even clear that it has created any new ones." A significant letter to the editor in the journal "The Mathematical Intelligencer" putting the field of fractals in a somewhat unfavorable light was then contributed by Brooks (*10*), who was a coworker with Mandelbrot on many early fractal endeavors. An article entitled "Fractal Fracas" appeared in "Science" and summarized (as of 1990) the controversy over fractal geometry (*40*). Among the topics discussed was the consensus of the mathematical community over the "legitimacy" of fractals. Axler (*4*), publisher of the "The Mathematical Intelligencer," stated that a majority of the mathematicians line up against the proponents of fractal geometry.

The authors' involvement with fractals has focused on computing the fractal dimension of profile traces and trying to use that dimension as a measure of roughness. Results have been disappointing, particularly with regard to the anomalies between the various fractal algorithms. These efforts could be easily dismissed by stating that the profiles were neither self-similar nor self-affine, thus implying that the fractal dimension was a redundant exercise. However, establishing the properties of self-similarity or self-affinity is difficult, particularly for empirical data.

In his Ph. D. thesis, Piggott (*39*, p. 115) used statistical, geostatistical, and fractal methods as measures of the roughness of a number of different surface profiles. The author concluded "that statistical and geostatistical analyses are the most appropriate means of quantifying fracture surface topography under the experimental conditions described in this chapter. Used in conjunction, the procedures describe both the statistical and spatial distribution of surface elevation in a manner amenable to analytical modelling of fracture properties. Fractal and spectral methods may yield superior descriptions of surface topography under different experimental conditions."

Some other authors who have enjoyed success using the fractal dimension postulate that the profiles are self-affine, rather than attempting to prove that this condition exists. Other users of fractal geometry seem to implement the technique without consideration of self-similarity or self-affinity. Based on the preceding discussion, the authors

recommend that future researchers should carefully weigh the pros and cons of the fractal geometry controversy before making their research commitments.

CONTINUING RESEARCH

Three research efforts using fractal dimensions are continuing at SRC. In photogrammetry, it is imperative to measure its effectiveness relative to larger scale situations. For this reason, a field study program will begin soon, using photogrammetry first on rock outcrops, then on rock surfaces underground.

Three-dimensional fractal analysis is a second area of interest. While there are several algorithms available for two-dimensional profile work, three-dimensional algorithms are scarce. One such algorithm requires even spacing in the x-y plane; the data are not amenable to this condition.

Estimated semivariogram functions have been used to obtain fractal dimensions for rock fracture profiles (*39*), where it is assumed that the roughness profiles are modeled effectively with a self-affine fractal model. In such cases, a log-log plot of the semivariogram yields data amenable to linear regression. The slope b of the regression line is then used to estimate D using the formula $D = 2 - b/2$.

Because semivariograms also can be used for surfaces, a topological D, rather than a profile D, is available. For the topological D, the formula is

$$D = 3 - b/2.$$

Work is progressing along these lines, with the goal being to obtain an estimate of the fractal dimension of the entire fractal surface while also investigating anisotropic properties of surface roughness.

Finally, another two-dimensional profile of a fractal dimension algorithm is being investigated. This method, called the variation method, is attributed to Dubuc, Roques-Carmes, Tricot, and Zucker (*19*). These authors claim that the variation method is superior to the algorithms described in the present RI. The variation method involves dividing the x-axis of the data into sets of bins, choosing a set of intervals about the bin centers, computing maximum and minimum z-values in the intervals, summing the differences between corresponding maximum-minimum values, and obtaining a fractal dimension from an ensuing log-log plot. The initial computer programming has been completed, but reliable reportable results are not available at this time.

SHEAR STRENGTH ESTIMATION

INTRODUCTION

Using the results obtained from analyzing the gneiss x-direction series of profiles, it was decided to attempt to model shear strength as a function of three parameters: fractal dimension, fractal intercept obtained by the modified divider algorithm, and Myers' Z_2 measure. These parameters were selected because of their high correlations with the visual rankings of the profiles (table 10).

Roughness profiles from six clean fractures were digitized using close-range photogrammetry and automated stereo digitizing. Two of the fractures were contained in basalt specimens, two in gneiss specimens, and two in quartzite specimens. The rock specimens were trimmed to be approximately 8 cm on a side, making the roughness profiles 6 to 7 cm in length. This size was appropriate for subsequent casting of the specimens with quick-setting cement to produce testable direct-shear specimens. Ten parallel roughness profiles were digitized in each of two directions, identified as the x- and y-directions. Thus, 20 profiles were obtained from each specimen, making a total of 120 profiles. To avoid generating excessively large amounts of data, the regular digitizing interval was approximately 0.2 mm, which produced about 300 observations along each profile. Figures 5 and 6 show the roughness profiles for the samples.

The estimated roughness measures were averaged for each set of 10 parallel profiles (table 16). Autocorrelation calculations for each of the roughness measures indicated that adjacent profiles (spaced about 5 mm apart) were independent of each other with regard to estimated roughness. This confirmed earlier results regarding the independence, variability, and uniqueness of adjacent profiles, implying that it would be difficult to select one single profile as representative of the entire fracture surface.

DIRECT-SHEAR TESTING

The six specimens containing the natural fractures were sheared with a direct-shear apparatus in SRC laboratories at a rate of 0.3 mm/min. Applied normal stresses were purposely kept low (i.e., less than 25 mt/m^2) to avoid extensive damage to fracture surfaces. Each specimen was sheared at six normal loads in the x-direction and six in the y-direction. Then one of the directions was selected for shearing at slightly higher normal stresses (i.e., up to about 80 mt/m^2).

Table 16.—Summary of averaged roughness measures and results of direct-shear tests for six fractures

Fracture	Direction	Averaged roughness measures			Direct-shear tests, peak strength envelope[1]		
		D	Intercept	Z_2	A	B	ϕ^0
			BASALT				
1	x	1.228	3.917	0.338	2.1060	0.9119	58.3
1	y	1.286	3.953	.278	1.7661	.9656	58.1
2	x	1.276	3.753	.451	1.5986	.8814	47.1
2	y	1.168	3.926	.257	1.7591	.8590	48.0
			GNEISS				
1	x	1.185	3.632	0.153	1.9481	0.7139	40.4
1	y	1.211	3.686	.143	2.1583	.7393	45.1
2	x	1.208	3.728	.258	1.6723	.7827	43.1
2	y	1.168	3.709	.143	2.0555	.7842	48.9
			QUARTZITE				
1	x	1.212	3.582	0.149	2.2478	0.7277	44.9
1	y	1.146	3.728	.153	2.2544	.7606	47.9
2	x	1.254	3.859	.327	1.9678	.8073	48.0
2	y	1.154	3.854	.196	2.2224	.8083	51.8

A, B Curve parameters.
D Fractal dimension.

[1]Power model is $\tau = A\,\sigma_n^B$; friction angle ϕ^0 is based on linear envelope.

Output from a shear test can be displayed as a graph with shear load plotted against shear displacement (fig. 10*A*). Using the peak shear strength observed for each trace, the laboratory data were reduced to provide estimates of shear-strength t as a function of normal stress σ_n (fig. 10*B*). In most situations, a nonlinear power curve provided a better model for describing the shear-strength envelope than did a linear model. This result concurs with observations previously published by Jaeger (*28*) and Miller and Borgman (*35*). Shearing direction had a significant influence on shear strength in the gneiss and quartzite samples. Results of the laboratory testing and model fitting are summarized in table 16.

As part of the laboratory work, a Schmidt L-hammer was used to take several measurements of hardness (i.e., joint wall compressive strength) on the surface of each of the fractures. These measurements then were averaged for each fracture and compared across the three rock types. Because there was so little variability among the results (values ranged from 36 to 44 on the hardness index), it was concluded that hardness could be considered uniform for all these specimens and could be ignored in subsequent analyses aimed at predicting shear strength. Thus, fracture roughness in conjunction with applied normal stress seemed to be the principal input needed to estimate peak shear-strength envelopes for such fractures.

SHEAR STRENGTH ESTIMATES FROM ROUGHNESS MEASURES

The initial goal of this project was to predict shear-strength envelopes as a function of roughness, hardness, and applied normal stress. As discussed above, fracture hardness was dismissed as having any significant influence on the specimens being studied here. This left three roughness measures to be considered: the fractal dimension (obtained from the slope of the log-log fractal plot), the y-intercept from the log-log fractal plot, and the Z_2 measure.

To investigate basic relationships between each roughness measure and each of the nonlinear shear-strength envelopes (estimated from the direct-shear tests), correlation coefficients were computed and then correlation matrix (table 3) was constructed based on the 12 direct-shear tests of the 6 fractures (tables 10 and 16). These correlation values indicated that the roughness measures significantly influenced the shape parameters of the strength envelopes (fig. 10) and that D and the Z_2 measure were significantly negatively correlated. (Recall that a correlation coefficient of 1.0 indicates perfect positive correlation, while -1.0 indicates perfect negative correlation in a linear sense.) If the median or the maximum value of the roughness measures were used for each set of

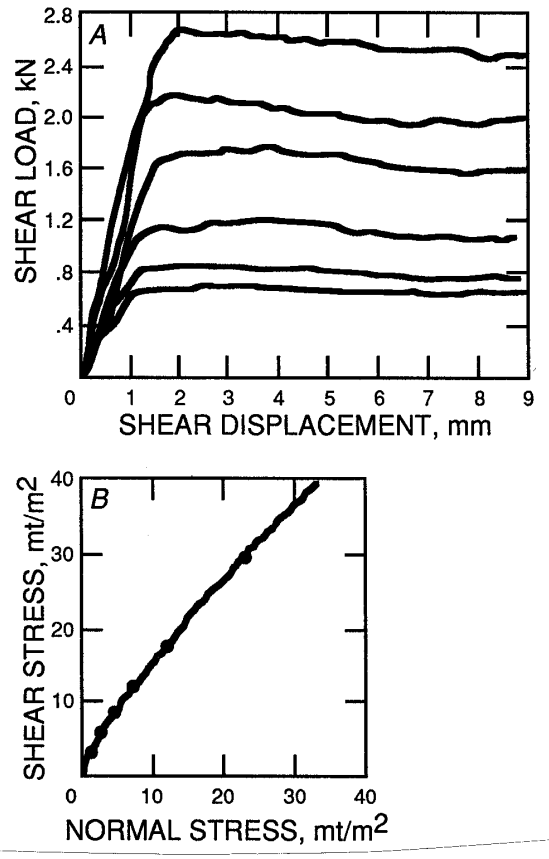

Figure 10.—Examples of direct-shear test results. Each trace represents application of a specified normal load. *A*, Plot of shear load as a function of shear displacement; *B*, peak shear-strength envelope fitted to test data, where $\tau = A\,\sigma_n^B$. (τ = shear stress; A and B = curve parameters; and σ_n = normal stress.)

10 parallel profiles instead of mean value, results were similar (table 3).

Some correlation was shown between the curve parameters A and B, but not enough to discourage the use of these parameters as independent terms in subsequent least squares regression modeling. The following linear regression models were applied to the data set:

$A = P_0 + P_1D$	$B = P_0 + P_1D$
$A = P_0 + P_1I$	$B = P_0 + P_1I$
$A = P_0 + P_1Z_2$	$B = P_0 + P_1Z_2$
$A = P_0 + P_1D + P_2I$	$B = P_0 + P_1D + P_2I$
$A = P_0 + P_1D + P_2I + P_3Z_2$	$B = P_0 + P_1D + P_2I + P_3Z_2$

where P_i = *i*th regression coefficient

and I = fractal intercept.

The latter two models represent general "hyperplanes" in multidimensional space. The merit of each model was judged using an index of determination R_I, which is analogous to the coefficient of determination (i.e., squared correlation coefficient) for simple linear regression. This index can be defined as follows:

$$R_I = 1 - \frac{\sum (y_i - \hat{y}_i)^2}{\sum (y_i - \bar{y}_i)^2},$$

where y_i = measured value of dependent variable,

$\hat{y}_i$ = value of dependent variable estimated from regression model,

and $\bar{y}$ = mean value of dependent variable.

None of the models showed an index greater than 0.6 for both A and B predictors except the model in which all three roughness measures were used. This model's indices were 0.625 for the A model and 0.765 for the B model.

Thus, based on the 12 direct-shear tests of clean fractures at low normal stresses, the curve parameters A and B for the shear-strength envelope $\tau = A\sigma_n^B$ can be estimated from the roughness measures, where A = 4.295 - 1.022 (D) - 0.201 (I) - 1.352 (Z_2), and B = -1.449 + 0.568 (D) + 0.412 (I) + 0.076 (Z_2).

In developing such models for the experimental data set, it was observed that the fractal intercept is at least as important as the fractal dimension for describing surface roughness and its subsequent influence on the shear strength of clean fractures.

To evaluate the effectiveness of these models, they were used to generate synthetic shear-strength envelopes and then to compare these envelopes with the actual envelopes produced by laboratory direct-shear tests. Examples are presented in figure 11 for two of the fractures. Both generated envelopes seemed reasonably compatible with actual envelopes, although the generated envelopes tended toward a hypothetical "mean" envelope for all tests considered here.

In testing for the influence of roughness on shear strength, equations of the form $\tau = P_1D\left(\sigma_n^{P_2D}\right)$ were also considered. The successful estimation of the coefficients P_1 and P_2 by nonlinear least squares regression demonstrated that fractal measures can be used to predict shear-strength envelopes. However, the sparseness of data by rock type in this particular study prevented pursuing these particular models.

Thus, it can be seen that nonlinear, power-curve-type, shear-strength envelopes for natural rock fractures can be predicted using three objective roughness measures:

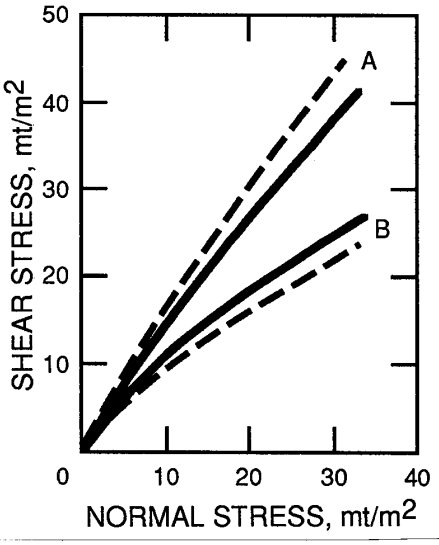

Figure 11.—Generated synthetic (solid line) versus actual (dashed line) peak shear-strength envelopes for two natural rock fractures. (A = basalt and B = gneiss.)

fractal dimension, fractal intercept, and the Z_2 measure. Two important observations were made in the early stages of the study:

1. Parallel profiles of fracture roughness are independent of each other when spaced as closely as 5 mm apart (implying the difficulty of selecting one particular profile to represent the entire topography of a surface). Even averaging the results from several parallel profiles may not provide representative roughness measures for a fracture surface.
2. Shear strength along natural fractures is often an anisotropic property (i.e., shear strength can depend on direction of shearing).

Use of the average (i.e., arithmetic mean), the median, and the maximum roughness measures for a set of parallel profiles was also investigated, but all yielded comparable correlations with strength envelope parameters. In addition, none of these two-dimensional measures was deemed entirely satisfactory as a representative roughness value for a given fracture surface.

CONCLUSIONS

The photogrammetric method of collecting and digitizing information from rock surfaces proved to be quite successful. Although not as precise as a mechanical profilometer, photogrammetry is accurate enough for many situations. Additional studies should involve large-scale surfaces underground.

Photogrammetry equipment is field portable. Photogrammetry and subsequent stereo digitizing can produce reasonable estimates of fracture roughness measures, as well as permanent records of fracture surfaces that can be readily profiled in any direction or topographically mapped to generate detailed digital elevation models. These data characteristics make it possible to analyze three-dimensional properties of rock fracture roughness. This analysis includes descriptions of anisotropy based on two-dimensional covariance and/or spectral analysis or on surface fractals rather than on profile fractals. Such studies can eliminate the uncertainty and possible errors in using only a few profiles (which often may not be representative) to characterize the roughness of an entire fracture surface.

A shear strength model was developed using the x-direction data from the surface of a gneiss sample. It is quite possible that a different model would have evolved if both x- and y-direction input had been processed. In spite of using only one direction, however, the resulting shear strength model did a good job of curve fitting the available shear strength data from 12 samples—4 gneiss, 4 basalt, and 4 quartzite. It was unfortunate that the hardness parameter proved to be insignificant when the available rock specimens were described; it was hypothesized that both parameters—roughness and hardness—would have generated a better model for shear strength computations than the model in which only roughness was used.

The major focus of this work was to find a single parameter as a measure of the roughness of a rock fracture surface. This effort led to detailed analyses of four fractal dimension algorithms—box, divider, modified divider, and spectral. Of these algorithms, the modified divider was the easiest to implement and provided the best agreement with generated profiles of known fractal dimension. The spectral method proved to be least dependable. Both the divider and box methods required parameter adjustments for proper implementation. When applied to a family of profiles, the intercorrelations between the four fractal measures proved to be disappointing. Furthermore, when compared to visual perceptions as to degree of roughness for a family of profiles, there was again a lack of consistency. The Z_2 measure was also computed throughout the analysis, but Z_2 alone was not sufficient to describe roughness. Although falling short of some of the

project's goals, such as establishing a unique measure of roughness, the authors feel that alerting the scientific community to some of the shortcomings of the fractal approach was a worthwhile endeavor, for such a detailed comparison of algorithms to empirical data has not been previously reported in the literature.

REFERENCES

1. American Society of Photogrammetry (Falls Church, VA). Close-Range Photogrammetry and Surveying: State of the Art. 1984, 941 pp.

2. Anderson, T. The Statistical Analysis of Time Series. Wiley, 1971, 326 pp.

3. Aviles, C. A., C. H. Scholz, and J. Boatwright. Fractal Analysis Applied to Characteristic Segments of the San Andreas Fault. J. Geophys. Res., v. 92, 1987, pp. 331-344.

4. Axler, S. The Mandelbrot Set, Fractals. Sec. in Letters to the Editor. Math. Intelligencer, v. 12, No. 1, 1990, pp. 3-5.

5. Barnsley, M. F., R. L. Devaney, B. B. Mandelbrot, H.-O. Peitgen, D. Saupe, and R. F. Voss. The Science of Fractal Images. Springer, 1988, 325 pp.

6. Barton, C., and E. Larsen. Fractal Geometry of Two-Dimensional Fracture Networks at Yucca Mountain, Southwestern Nevada. Paper in Proceedings of the International Symposium on the Fundamentals of Rock Joints. Bjorkliden, 1985, pp. 77-84.

7. Barton, N. Review of a New Shear Strength Criteria for Rock Joints. Eng. Geol., v. 7, 1973, pp. 287-332.

8. Barton, N., and V. Choubey. The Shear Strength of Rock Joints in Theory and Practice. Rock Mech., v. 10, 1977, pp. 1-54.

9. Bendat, J. S., and A. G. Piersol. Random Data: Analysis and Measurement Procedures. Wiley, 2d ed., 1986, 566 pp.

10. Brooks, R. The Mandelbrot Set. Sec. in Letters to the Editor. Math. Intelligencer, v. 12, No. 12, 1990, p. 3.

11. Brown, S. R. Fractal Dimension of Rough Surfaces and Some Geophysical Records. Sandia Laboratories, Sandia, NM, Tech. Rep. SAND89-1934j, 1989, 17 pp.

12. ____. A Note on the Description of Surface Roughness Using Fractal Dimension. Geophys. Res. Lett., v. 14, 1987, pp. 1095-1098.

13. Brown, S. R., and C. H. Scholz. Broad Bandwidth Study of the Topography of Natural Rock Sources. J. Geophys. Res., v. 90, 1985, pp. 12575-12582.

14. Brownlee, K. A. Statistical Theory and Methodology. Wiley, 1965, 590 pp.

15. Carr, J. R., and J. B. Warner. Rock Mass Classification Using Fractal Dimensions. Paper in 28th U.S. Symposium on Rock Mechanics, ed. by I. Farmer (Proc., Univ. AZ, Tucson, AZ, 1987). Balkema, 1987, pp. 73-80.

16. Chiles, J. P. Fractal and Geostatistical Methods for Modeling of a Fracture Network. Bur. de Recher. Geol. et Minieres, BP 6009, 1988, 29 pp.

17. Coughlin, J., and R. Kranz. New Approaches To Studying Rock Burst-Associated Seismicity in Mines. Paper in Rock Mechanics as a Multidisciplinary Science: Proceedings of the 32nd U.S. Symposium, ed. by J.-C. Roegiers (Univ. OK, Norman, OK, July 10-12, 1991). Balkema, 1991, pp. 491-500.

18. Dixon, W. J., and F. J. Massey. Introduction to Statistical Analysis. McGraw-Hill, 3d ed., 1969, pp. 111-121.

19. Dubuc, B., C. Roques-Carmes, C. Tricot, and S. W. Zucker. The Variation Method: A Technique To Estimate the Fractal Dimension of Surfaces. Proceedings, Visual Communications and Image Processing II. Int. Soc. Optic Eng., v. 845, 1987, pp. 241-248.

20. Feder, J. Fractals. Plenum, 1988, 283 pp.

21. Ferrero, A. M., and G. P. Giani. Geostatistical Description of Joint Surface Roughness. Paper in Rock Mechanics Contributions and Challenges: Proceedings of the 31st U.S. Symposium, ed. by W. A. Hustrulid and G. A. Johnson (CO Sch. Mines, Golden, CO, June 18-20, 1990). Balkema, 1990, pp. 463-470.

22. Fox, C. G. Empirically Derived Relationships Between Fractal Dimensions and Power Law Form Frequency Spectra. Pure and Appl. Geophys. (PAGEOPH), v. 131, No. 1/2, 1989, pp. 212-239.

23. Ghosh, S. K. Analytic Photogrammetry. Pergamon, 2d ed., 1988, 308 pp.

24. Gilbert, L. E. Are Topographic Data Sets Fractal? Pure and Appl. Geophys. (PAGEOPH), v. 131, No. 1/2, 1989, pp. 242-254.

25. Hough, S. E. On the Use of Spectral Methods for the Determination of Fractal Dimension. Geophys. Res. Lett., v. 16, 1989, pp. 673-676.

26. International Society for Rock Mechanics, Commission on Standardization of Laboratory and Field Tests. Suggested Methods for the Quantitative Description of Discontinuities in Rock Masses. Int. J. Rock Mech. and Min. Sci. & Geomech. Abstr., v. 15, 1978, pp. 319-368.

27. Isaaks, E. H., and R. M. Srivastava. Spatial Continuity Measures for Probabilistic and Deterministic Geostatistics. Math. Geol., v. 20, 1988, pp. 313-341.

28. Jaeger, J. C. Friction of Rocks and Stability of Rock Slopes. Geotechnique, v. 21, 1971, pp. 97-134.

29. Korvin, G., D. M. Boyd, and R. O'Dowd. Fractal Characterization of the South Australian Gravity Station Network. Geophys. J. Int., v. 100, No. 3, 1990, pp. 535-539.

30. Krantz, S. G. Fractal Geometry. Math. Intelligencer, v. 11, No. 4, 1989, pp. 12-16.

31. Lee, Y.-H., J. R. Carr, D. J. Barr, and C. R. Haas. The Fractal Dimension as a Measure of the Roughness of Rock Discontinuity Profiles. Int. J. Rock Mech. and Min. Sci. & Geomech. Abstr., v. 27, No. 6, 1990, pp. 453-464.

32. Mandelbrot, B. B. The Fractal Geometry of Nature. Freeman, 1983, 468 pp.

33. ____. Some Facts That Evaporate Upon Examination. Math. Intelligencer, v. 11, No. 4, 1989, pp. 17-19.

34. McWilliams, P. C., J. C. Kerkering, and S. M. Miller. Fractal Characterization of Rock Fracture Roughness for Estimating Shear Strength. Paper in Mechanics of Jointed and Faulted Rock, ed. by H. P. Rossmanith (Proc. Int. Conf. on Mech. of Jointed and Faulted Rock, Vienna, Austria, Apr. 18-20, 1990). Balkema, 1990, pp. 331-336.

35. Miller, S. M., and L. E. Borgman. Probabilistic Characterization of Shear Strength Using Results of Direct Shear Tests. Geotechnique, v. 34, 1984, pp. 263-276.

36. Miller, S. M., P. C. McWilliams, and J. C. Kerkering. Evaluation of Stereo Digitizing for Measuring Rock Fracture Roughness. Paper in Rock Mechanics as a Guide for Efficient Utilization of Natural Resources: Proceedings of the 30th U.S. Symposium, ed. by A. W. Khair (WV Univ., Morgantown, WV, June 19-22, 1989). Balkema, 1989, pp. 73-80.

37. ____. Ambiguities in Estimating Fractal Dimensions of Rock Fracture Surfaces. Paper in Rock Mechanics Contributions and Challenges: Proceedings of the 31st U.S. Symposium, ed. by W. A. Hustrulid and G. A. Johnson (CO Sch. Mines, Golden, CO, June 18-20, 1990). Balkema, 1990, pp. 471-478.

38. Myers, N. O. Characterization of Surface Roughness. Wear, v. 5, 1962, pp. 182-189.

39. Piggott, A. R. Analytical and Experimental Studies of Rock Fracture Hydraulics. Ph.D. Thesis, PA State Univ., University Park, PA, 1990, 252 pp.

40. Pool, R. Fractal Fracas. Science, v. 249, 1990, pp. 363-364.

41. Rayner, J. N. An Introduction to Spectral Analysis. Pion (London), 1971, 174 pp.

42. Seigel, S. Nonparametric Statistics. McGraw-Hill, 1956, pp. 213-223.

43. Smalley, R. F., J.-L. Chatelain, D. L. Turcotte, and R. Prevot. A Fractal Approach to the Clustering of Earthquakes: Applications to the Seismicity of the New Hebrides. Bull. Seismol. Soc. Am., v. 77, No. 4, 1987, pp. 1368-1380.

44. Tse, R., and D. M. Cruden. Estimating Joint Roughness Coefficients. Int. J. Rock Mech. and Min. Sci. & Geomech. Abstr., v. 16, 1979, pp. 303-307.

45. Turcotte, D. L. Fractals and Fragmentation. J. Geophys. Res., v. 91, No. 82, 1986, pp. 1921-1926.

46. Wong, P. Fractal Surfaces in Porous Media. Paper in Proceedings 154. Amer. Inst. of Phys., 1987, pp. 304-318.

47. Wu, T. H., and E. M. Ali. Statistical Representation of Joint Roughness. Int. J. Rock Mech. and Min. Sci. & Geomech. Abstr., v. 15, 1978, pp. 259-262.

48. Yfantis, E. A., G. T. Flatman, and E. J. Englund. Simulation of Geological Surfaces Using Fractals. Math. Geol., v. 20, No. 6, 1988, pp. 667-672.

APPENDIX A.—PROCEDURES FOR CLOSE-RANGE PHOTOGRAMMETRY

SPECIMEN DESCRIPTION

For the photogrammetric work in the laboratory, three different rock types were used: basalt, gneiss, and quartzite. These types were chosen primarily because of convenience; they are the most readily available rock types in the area. Sedimentary rocks were excluded solely because there are no sedimentary formations in northern Idaho and eastern Washington.

Two specimens of each rock type were collected, each containing a natural fracture. The specimens were then trimmed to 8- by 9- by 3-cm blocks having 1.5 cm of intact rock on either side of the fracture. This yielded 12 samples (6 pairs of mated halves). The 12 trimmed and fractured specimens were then cast in quick-setting cement in a 10- by 10-cm mold to produce samples for direct-shear tests.

EQUIPMENT FOR CLOSE-RANGE PHOTOGRAMMETRY

The use of close-range photogrammetry was suggested by an article describing the successful use of this technique to measure wear on asphalt roads in California (*1*, pp. 530-551).[1] Although the highway project involved the use of two 35-mm cameras to take the photographs, only specialized photogrammetric cameras or cameras that had been specially calibrated for photogrammetric work were considered because the Bureau project required more precise measurements.

Two Rollei[2] single-lens reflex cameras with 80-mm Zeis lenses and two 34-mm-long extension tubes (fig. A-1) were selected. An 80-mm lens can focus to 1 m, which covers a viewing area 50 by 50 cm. By using an extension tube, the distance between the camera and the specimen could be narrowed to 38.5 cm, covering an area of 10 by 10 cm and enabling the image of the specimen to fill the frame. The extension tube and the lens had to be calibrated together at this distance.

To provide support for the two cameras, a 3-ft by 2- by 1/4-in aluminum bar was milled with a 1/4-in slot cut part way down the middle; the cameras were then bolted to the bar by 1/4-in screws passing through the slot in the bar to a tripod-mounting hole on the cameras. The slot allowed the distances between the cameras to be adjusted as desired. The bar was then bolted to the top of the sturdiest tripod available. The importance of the sturdiness of the tripod cannot be overemphasized. Any shaking in the cameras when taking the pictures will result in blurry photographs, which will compromise the accuracy of the gathered data. A cable release is also recommended to help minimize camera shake.

Sometimes small mounts containing rack-and-pinion gears allowing movement in both the x- and y-directions are helpful for fine tuning camera positions. The cameras are first attached to these mounts and then bolted to the aluminum bar. For photographing in the laboratory, a second tripod is handy for holding the specimen and its reference frame. The tripods should have a rack-and-pinion shaft to enable fine adjustments. This permits raising or lowering either the cameras or the specimen to obtain the desired framing.

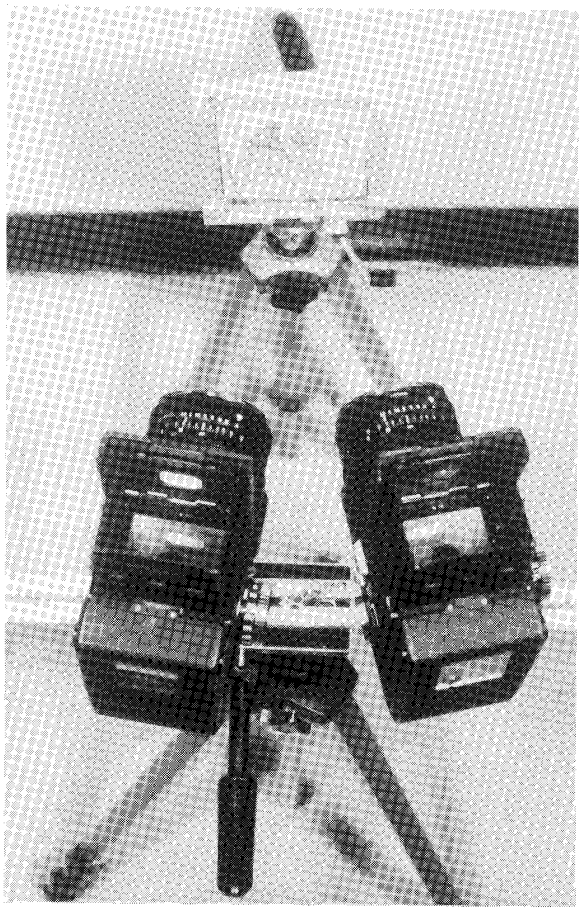

Figure A-1.—Photogrammetric setup showing two Rollei cameras mounted on support bar and rock specimen mounted in aluminum reference frame.

[1]Italic numbers in parentheses refer to items in the list of references preceding this appendix.

[2]Reference to specific products does not imply endorsement by the U.S. Bureau of Mines.

Photogrammetry requires both horizontal and vertical control in the picture area. This control allows calibration of the digitizing and plotting equipment. For the laboratory samples, a 12- by 12-cm aluminum reference frame was fabricated. This frame had a 10-cm-square opening to allow insertion of the sample. Inscribed on the frame every few centimeters were crosshairs. These provided horizontal control. The corners of the frame were elevated by approximately 1 cm to help provide vertical control. In addition, a 1-cm cube was attached to the frame for further vertical control.

Color slide film (Ektachrome ASA 100) was used instead of negative film. The information was read directly from the positive slide images, and it was felt that this gave better resolution than converting negative film into prints and then analyzing the prints. The colored image also helped to obtain more accurate readings.

EQUIPMENT CALIBRATION

Usable cameras for photogrammetry are either metric or nonmetric. (Here, "metric" means measured.) The metric camera is constructed with either fiduciary marks (marks inside the camera on the film plane that show on the negative) or a Reseau plate. The Reseau plate sits in the light path immediately in front of the film plane and has a grid on it that shows on the exposed film. Both fiduciary marks and the Reseau plate serve the purpose of helping to determine the amount of distortion in the film caused by buckling.

A metric camera also comes with a scale that shows lens distortion at various focusing distances; it may also be equipped with a vacuum film back to hold the film perfectly flat against the platen. Such cameras as the Hasselblad MK70 are quite expensive, costing in excess of $20,000 for just the body and lens.

Nonmetric cameras are not equipped with specialized equipment or scales of measurement. Examples are Hasselblad or Rollei cameras in the 70-mm^2 format or Nikon, Pentax, or Leica cameras in the 35-mm format. These cameras need to be calibrated to be suitable for precise photogrammetry, which, if contracted out, can cost up to $1,000.

Nonmetric cameras were chosen because they cost much less than metric cameras, even with the necessity of calibrating them. Nonmetric cameras can also be used for ordinary photography, thus saving the cost of additional photographic equipment for another research project.

The calibration procedure requires first engraving fiduciary marks on the four corners of the film plane. These marks serve in place of the Reseau plate.

Lens distortion must be measured at each planned picture-taking distance. At each position, the radial and tangential distortions are measured, and this information is later entered into the computer program used to run the analytic plotter. This enables the plotter to compensate automatically for lens distortion and unevenness of the film.

An analytic self-calibration computer program that enables individuals to calibrate their own camera systems is included in reference 23. This reference also includes sample input and output.

PHOTOGRAPHIC PROCEDURES

The following procedure was used for taking photogrammetric pictures in the laboratory. The cement part of the specimen block was clearly marked as to top, bottom, left, and right and then placed in the aluminum reference frame. The block and frame were mounted vertically on a small platform attached to the top of a tripod. The two Rollei cameras were mounted on the rack-and-pinion gears attached to the aluminum bar and this bar was attached to the top of another tripod (see figure A-1). The cameras were moved back and forth on the bar until each camera had the same image and image size. The angle of inclination was also checked to ensure that it was the same for both cameras.

This setup procedure was greatly facilitated by using a measuring tape to determine the distance from the top center front of the reference frame to the film plane of each camera. These distances should be equal. The height (horizontal distance) from the top center front of the reference plane to an imaginary line connecting the film planes of the two cameras was also measured. This distance was a common side of two right triangles and so was used to calculate the actual measured distances.

Two lights with daylight bulbs were positioned horizontally and vertically at 45° angles on each side of the specimen. The lights were placed at equal distances from the specimen to ensure uniform lighting. All other lights in the room were turned out and the windows were darkened. This ensured the correct color balance on the specimen and helped maintain surface relief, which would have been smoothed by light from extraneous sources.

The cameras were tripped successively by means of cable releases to minimize vibrations. The mirrors on each camera were locked upright to further reduce picture fuzziness caused by camera vibrations.

A spot meter and gray card were used to determine light levels and exposure information. Light meter readings were taken from the gray card held immediately in front of the specimen. This combination was also used to check the evenness of the light intensity on different parts of the sample. These readings were compared with spot readings taken directly off the face of the sample.

The shutter f-stop combination was chosen to give the maximum depth of field. Generally, the combination was

f22 or f16 at 1/15th of a second. Several combinations were used on each specimen, but each pair of pictures was always taken with the same combination.

PHOTOGRAPH PROCESSING BY ANALYTIC PLOTTER

Use of an analytic plotter made the photogrammetric approach possible. Without photogrammetry, it would have been too time consuming and expensive to measure the required number of points on a rock surface (over 80,000 sets on a 9- by 9-cm surface). Such massive amounts of data could not have been generated using older mono and stereo comparators, which plot just one profile at a time. The analytic plotter allows the x, y coordinates of a profile and the density of points along the profile to be set. The readings are recorded automatically, requiring an operator simply to set the initial conditions and monitor the process.

The profiles were plotted with 40-μm (0.04-mm) dots. This size is almost as large as the space between adjacent points, which makes it difficult to understand how points closer than one-half of 40 μm can be measured. An experiment was conducted in which the original 70-mm negatives were enlarged 2.44 times to see if the enlarging process made a difference in the robustness of the data. This test is discussed in the section "Photographic Enlargements" in appendix B.

When the project was initiated, there were only a few firms in the continental United States with analytic plotters and only one firm in the Pacific Northwest, Spencer B. Gross, Inc., of Portland, OR. A procedure evolved in which color slides (positives) of the specimen in the control frame were sent to the firm along with measurements of the height (distance) of the cameras from the sample, the angle of convergence of the cameras, and the separation distance. The company ran the profiles using a Wild stereo analytic plotter, model Avilyt BC1, and returned the x, y, z coordinates of the points on 5-1/4-in floppy discs using the American Standard Code for Information Interchange (ASCII) format. The data were then processed.

In reading the profile data from the photographs, investigators tried to obtain the most precise measurements the equipment was capable of making, which turned out to be 0.05 mm between points and between heights. Points closer than 0.05 mm or differing in height by less than 0.05 mm were treated as the same point.

APPENDIX B.—EVALUATION OF CLOSE-RANGE PHOTOGRAMMETRY

ACCURACY ANALYSIS

Accuracy Bar

The purpose of an accuracy bar (fig. B-1) is to test photogrammetric results against a known standard. Knowing how photogrammetric results compare to a known standard enables better characterization of the accuracy of the complete system. The standard was a milled aluminum bar 10.2 cm long, 4 cm wide, and 2 to 2.5 cm high. Four tapered holes were drilled to various depths in the top. In addition, seven steps 2 to 4 mm high and 2 to 4 mm wide were cut into the surface to test how accurately depth was measured when photogrammetry was used. The test bar was photographed, and the photographs were digitally processed by Spencer B. Gross, Inc., Portland, OR. Each trace covered all the steps and one or more of the holes. Between the traces, the traces covered all the holes.

The same traces were sent to the University of Idaho, Moscow, ID, where they were measured with a mechanical transducer and with a metroplate and measuring dial with a long probe that penetrated to the bottom of the tapered holes and steps. Plots of one of the three traces depicting the three different measuring schemes are shown in figure B-2.

It was necessary to use an appropriate statistical test to determine if the three measuring processes were or were not equivalent. As the traces in figure B-1 indicate, it was not possible to match exactly the three reading positions on the horizontal axis. Therefore, to make reasonable comparisons of the three traces, the differences between the heights (z-values) at designated abscissas were compared (table B-1).

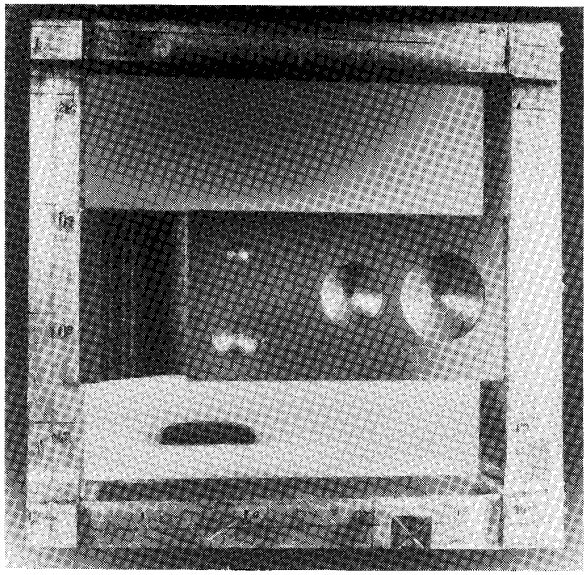

Figure B-1.—Accuracy bar in aluminum reference frame. Trace 1 runs through middle of bar encompassing two large holes and seven steps.

Table B-1.—Table of differences, millmeters

Photogrammetry	Mechanical transducer	Metroplate
	TRACE 1	
5.94	5.85	6.2
5.97	5.82	6.12
7.49	7.77	7.67
7.54	7.74	7.63
	TRACE 2	
0.02	0.02	0.005
1.30	1.41	1.4122
1.33	1.41	1.4046
.01	.03	.0025
	TRACE 3	
1.88	2.03	2.027
1.85	1.95	1.973
1.87	2.0	1.991
7.54	7.74	7.63
1.83	1.99	1.987
1.77	1.99	2.006
1.05	1.08	1.046
10.79	11.19	11.153
2.57	2.73	2.718
2.66	2.73	2.713

This process was possible even though the abscissa points did not exactly match. This was because the accuracy bar is uniformly flat, except for the steps and the drilled holes, and so the abscissa coordinates on a flat surface did not matter when determining the differences between measured heights of two differing-in-height flat surfaces.

A randomized block design analysis-of-variance model (*14*) was the statistical method used. Either by inspecting the data or using the ensuing F-statistic, it can be seen that the traces vary significantly from each other. The point of interest is to compare the three measuring procedures—photogrammetry, metroplate, and mechanical transducer. The resulting sample F-statistic of comparison is $F(2,39) = 3.04$. At the 0.95 significance level, the tabular F-statistic is 3.21. Because the sample statistic is less than the critical level statistic, the conclusion is that the three methods are not statistically different. Thus, photogrammetry is an acceptable method of data collection.

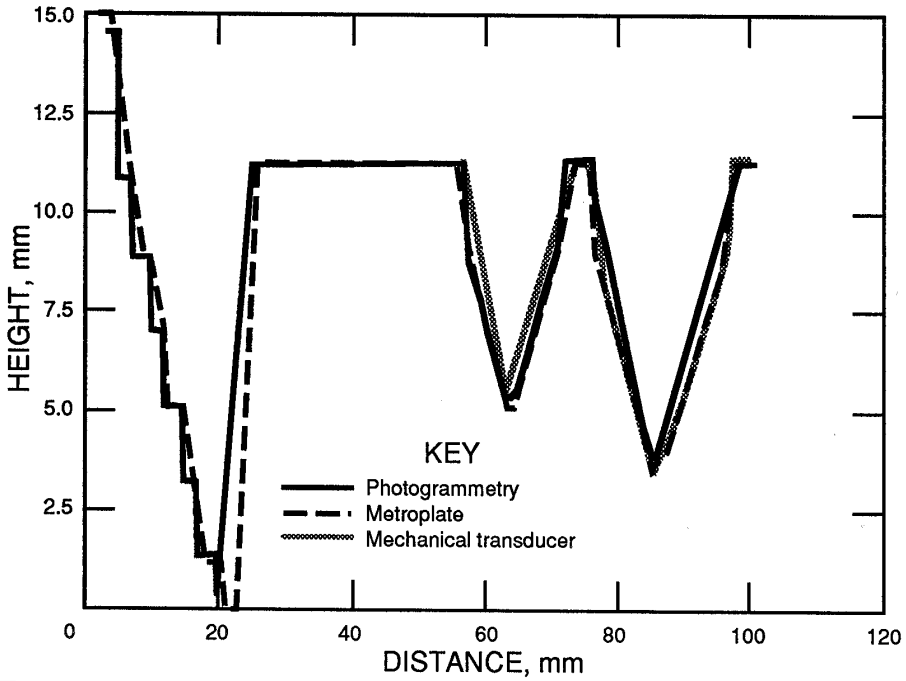

Figure B-2.—Three different measuring methods on trace 1 (middle trace) of accuracy bar.

Photographic Enlargements

In conducting geostatistical analyses of the profile data sets, unexplainable perturbations in the results were found. A possible reason was the size of the dot (40 μm) on the analytic plotter. The operator uses this dot to pick the points for digitizing. Because the sampling density was 0.05 mm, only 0.01-mm spaces were left between points, which could result in the same point being read for two different points. Thus, the data would be smoothed out, there would be less variability, and the roughness of the profile would be less.

To see if the dots were overlapping, a copy of a slide was enlarged 2.44 times from the original 2-1/4- by 2-1/4-in slide. This enlarged slide was then processed using the same profiles as on the original slide.

The enlarged slide was more convenient for the plotter operator to use, but did not necessarily generate more accurate measurements because of distortions introduced by the photographic process. The data were probably improved because of the easier pace of data sampling, which may minimize the perturbations seen in original data sets.

The results showed that indeed there was some smoothing of the data when the smaller slide was used (figure B-3 and table B-2). This smoothing, however, was not enough to affect the calculated values of the roughness measures in any significant way. For all practical purposes, then, the smaller slide was appropriate to use even at a point density of 0.05 mm.

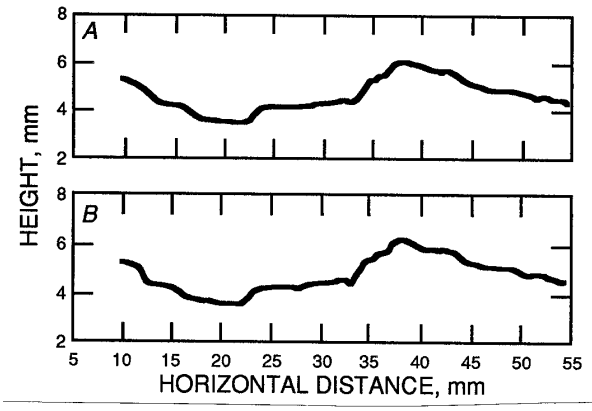

Figure B-3.—Comparison of profiles using original and enlarged slides. *A*, Profile of GHJ from original 2-1/4- by 2-1/4-in slide; *B*, profile of GEHJ from slide enlarged 2.44 times.

Table B-2.—Summary statistics comparing an original profile (GHJ) to its enlargement (GEXJ)

	GHJ	GEXJ
Data points in sample	873	896
Standard deviation[1]	.75146	.76746
Variance[1]	.564692	.588993
Standard deviation number[2]	.75103	.767031
Variance number[2]	.564045	.588336
Skewness	.134612	.129583

[1]Estimators for population using (n - 1).
[2]Estimators for sample using n.

COMPARISON OF PROFILOMETER AND PHOTOGRAMMETRY

For the initial investigation of photogrammetry, it was necessary to evaluate its usefulness and effectiveness as compared to more traditional ways of collecting data. To this end, a test procedure was set up and arrangements were made for Lawrence Livermore Laboratories of Livermore, CA, to measure profiles of a given sample. The profiles were then remeasured using the photogrammetric technique and the results from the two methods were compared.

Data Collection

For the comparative study, an irregularly shaped, silty quartzite specimen containing a natural fracture and trimmed to 8 by 9 by 3 cm was chosen. To facilitate the profilometric and photogrammetric studies (as well as future direct-shear tests), each half of the specimen was cast in quick-setting cement in a 10- by 10-cm mold, leaving an exposed fracture surface that could be measured for surface roughness. Only one of these fracture surfaces was analyzed during the study.

Profilometric Measurements

William Durham, a rock mechanics researcher who has been studying rock fracture topography as part of a larger investigation in fluid flow mechanics in fractured rock, supervised the profilometric measurements at Lawrence Livermore Laboratories. Technicians profiled four parallel traces spaced 2 cm apart in a defined x-direction (width) and four in a corresponding y-direction (length) using a profilometer. The tip of the profilometer stylus is semirounded and has a nominal width of approximately 0.0015 in. The tip leaves a faint "scribe" line on the fracture surface as each trace is profiled. These marks were used to align and register the stereo plotter so that the same eight traces could be digitized with photogrammetric methods.

Elevation measurements were taken at increments of 0.002 in (0.0508 mm) along each of the eight traces. The horizontal distance was recorded in inches, while the elevations were recorded as voltage generated by the stylus. Both types of measurements were subsequently converted to millimeters. Traces 1 to 4 in the x-direction were approximately 60 mm long, while traces 5 to 8 in the y-direction were approximately 70 mm long. The resulting profiles are presented in figure B-4.

Photogrammetry and Stereo Digitizing

The rock specimen was photographed at the Bureau's Spokane Research Center (SRC) under strict photogrammetric guidelines. The two cameras were aimed at the fracture surface at a convergence angle of 9.5° for each camera. The base distance between the midpoints of the two film planes was 128 mm. The perpendicular distance from each film plane to the center of the fracture surface was 385 mm, while the perpendicular distance from the baseline to the fracture surface was 380 mm. The 34-mm extension tubes made it possible to photograph the rock fracture surface at close range for maximum image size and to focus the lenses at infinity for concurrence with photogrammetric calibration factors. The exposure time was 1/125 s at f16.

The two sets of profiles (fig. B-4) had different starting coordinates arbitrarily located along a horizontal reference. To align, or register, a given pair of profiles, the horizontal coordinate corresponding to the minimum elevation on the stereo-digitized profile was matched to the same location on the profilometric profile. A new arbitrary horizontal axis was then defined. Using the new axis, the profiles were truncated, if necessary, so that each set of matched profiles had approximately the same beginning and ending points in the horizontal plane. Profiles were registered in the vertical plane by subtracting the mean elevation of a given profile from each of its recorded elevations and adding 5 mm. This resulted in all profiles being centered about an arbitrarily defined mean elevation of 5 mm.

Measurement Repeatability

During the profilometer exercise, profile 1 was digitized twice so that a replicate would be available to estimate measurement repeatability of the profilometer. All eight profiles were digitized twice with the stereo digitizer, although only profile 1 was used in the comparisons. Summary statistics for the absolute values of deviations (i.e., $|Z_1 - Z_2|$, where Z_1 and Z_2 = the corresponding elevations from the original trace and the replicate trace, respectively) are given in table B-3 and indicate that the

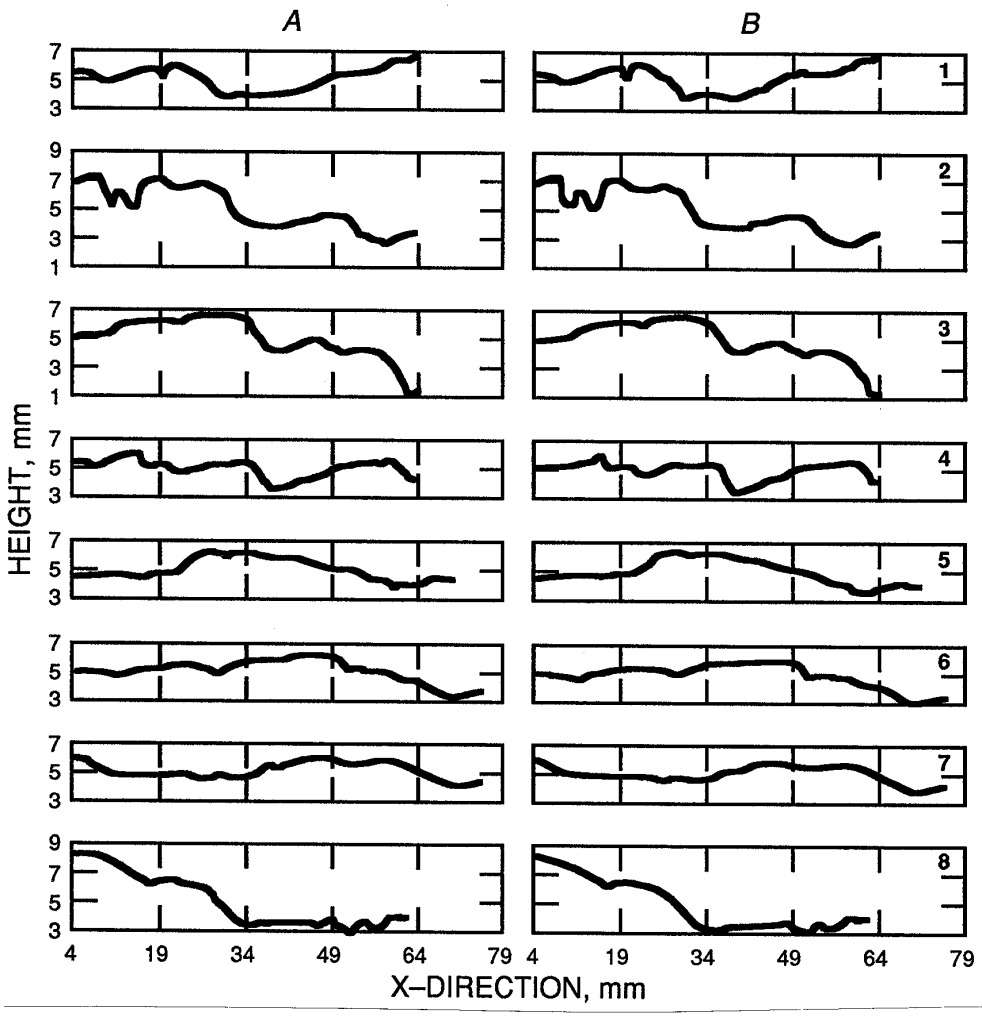

Figure B-4.—Roughness profiles for rock fracture surfaces at 2.5 times vertical exaggeration. Profiles 1-4 are in x-direction and profiles 5-8 are in y-direction. *A*, Profilometer results; *B*, photogrammetry results.

repeatability of the mechanical profilometer was approximately twice as good as that of the stereo digitizer. The quartile values and the relatively large standard deviations are representative of probability distributions skewed to the right.

Table B-3.—Summary statistics for absolute deviations in measured elevations obtained by repeating digitization of profile 1, millimeters

Method	Mean	Standard deviation	Lower quartile	Median	Upper quartile
Profilometer . .	0.012	0.013	0.0042	0.0082	0.0132
Stereo digitizer	.028	.033	.0057	.0157	.0357

The upper quartiles indicate that 75 pct of the absolute deviations from the mechanical profilometer were less than 0.0132 mm, whereas 75 pct of the absolute deviations from the stereo digitizer were less than 0.0357 mm. Thus, conservative estimates of measurement errors for the elevation data were approximately ±0.02 mm for the profilometer and ±0.04 mm for the stereo digitizer.

Comparisons of Roughness Data

One way of comparing the profile data obtained by the two different methods was to use a matched-pairs t-test on elevation data recorded along the same profile. However, because of the slightly different digitization interval used

in the two methods (0.002 in for the profilometer versus 0.05 mm for the stereo digitizer), it was impossible to match up any two corresponding points precisely. Furthermore, an inspection of the original profile data files showed that for any given profile, the horizontal increment was not a constant, but deviated slightly from the specified spacing. Thus, for comparative purposes, local means were computed in nonoverlapping neighborhoods (cells) approximately 0.6 mm wide, each of which contained about 12 original observations. Although this procedure provided smoothed elevation values, the new set of roughness observations was more compatible with the basic statistical assumptions of independence and normality upon which matched-pairs t-tests are based. In contrast, neither assumption was very well satisfied by the original roughness measurements; only three of the eight profiles had elevation data that approximated a normal distribution, and all profiles contained spatially dependent elevation data.

The matched-pairs t-test was conducted according to guidelines from Dixon and Massey (*18*, pp. 119-121). The value of the t-statistic is computed as follows:

$$t = \frac{(\bar{d} - o)}{\left(\frac{s}{\sqrt{n}}\right)},$$

where $\bar{d}$ = arithmetic mean of paired differences

$$= \frac{1}{n} \sum_{i=1}^{n} |(x_1 - x_2)_i|,$$

s = standard deviation of paired differences,

and n = number of paired differences (number of local means).

The null hypothesis, that the compared profiles were the same, would have been rejected if the calculated t-value exceeded 1.99, which is the critical value for typical n values at a significance level of 0.05. For each t-calculation, the corresponding probability of obtaining at least the absolute value of the t-statistic was also calculated. A high-probability value implied that the paired profiles were very similar.

Results from the matched-pairs analyses are given in table B-4 and indicate that for all eight profiles, there is negligible difference between the use of the profilometer or the stereo digitizer with regard to roughness data expressed as local means. This finding was further confirmed by linear regressions of the paired profile data, which yielded correlation coefficients greater than 0.98 in all cases. The repeatability trials shown in the last two rows of table B-4 imply that the stereo digitizer was better than the profilometer at reproducing consistent values of local means of the elevations along a profile.

Table B-4.—Matched-pairs comparisons of local means for roughness data obtained by mechanical profilometer (MP) and stereo digitizer (SD)

Matched profiles	Calculated t-statistic	Probability value	Linear correlation coefficient
MP1-SD1	0.02	0.9839	0.9928
MP2-SD2	-.04	.9657	.9810
MP3-SD3	.04	.9710	.9980
MP4-SD4	-.04	.9680	.9840
MP5-SD5	.03	.9800	.9929
MP6-SD6	.05	.9639	.9946
MP7-SD7	.04	.9644	.9910
MP8-SD8	0	.9998	.9926
MP1A-MP1B	.13	.8955	.9999
SD1A-SD1B	.04	.9719	.9985

To evaluate the influence of the size of the averaging window, the interval width was varied from about 0.4 mm (8 observations per cell) to 1.2 mm (24 observations per cell). The resulting t-values were small and did not significantly differ from those presented in table B-4.

A two-sample variance test (σ_1 versus σ_2) based on an F-statistic (*14*, pp. 285-286) also was applied to the roughness profiles. The null hypothesis would have been rejected if the calculated value ($F = \sigma_1/\sigma_2$) exceeded the critical F-value, which equaled 1.12 for n values typical of these profiles at a significance level of 0.05.

The variances and calculated F-value for the detrended data (table B-5) indicated that (1) variances from paired profiles were similar, but not strongly so; (2) roughness data generated by the stereo digitizer generally had smaller variances than data from the profilometer; (3) anisotropy was apparent in the fracture roughness, and the x-direction profiles were consistently rougher (i.e., higher variance) than the y-direction profiles; and (4) detrended roughness data provided a more reasonable basis for comparing profiles than did the raw data because variances in the raw data were influenced by trends.

Comparisons Based on Derived Roughness Measures

An empirical equation developed by Tse and Cruden (*44*) was applied to the profile data to estimate values of joint roughness coefficient (JRC). This procedure is based on the Z_2 measure (root mean square of the first derivative of the profile) (*38*) and relies on a digitization interval of 1.27 mm. To meet the interval requirement a cubic spline interpolation scheme was used to generate new elevation values at a constant spacing of 1.27 mm, which produced profiles with approximately 50 observations each. After computing the Z_2 for each profile, the empirical

equation JRC = 32.2 - 32.47 log (Z_2) was used to predict a JRC value (table B-6). With the exception of profiles 5 and 6, the stereo digitizer and the profilometer provided nearly identical JRC values. Also, the stereo-digitizer-derived JRC values generally were slightly less than those derived from the profilometer.

A deterministically derived, nonergodic covariance estimator ($\hat{C}$) was used to compute the geostatistical covariance of elevations along each of the profiles. This estimator [(adapted from Isaaks and Srivastava) (*27*)] is defined as:

$$\hat{C}(h) = \frac{1}{N(h)} \left[\sum_{i=1}^{N(h)} z(x_i)\, z(x_i + h) - \left[\sum_{i=1}^{N(h)} z(x_i) \right] \left[\sum_{i=1}^{N(h)} z(x_i) + h \right] \right],$$

where h = separation distance, or lag,

N(h) = number of sample pairs separated by lag h,

and z(x) = data value at location x.

The original definition of this estimator relied on spatial integrals and was an extension of earlier time-series work by Anderson (*2*); further explanations are beyond the scope of the current discussion. Suffice it to say that this covariance model has several mathematical advantages over traditional, probabilistic models of covariance (*27*), one of which is nonreliance on a stationary mean.

Elevation covariance was computed for each of the roughness profiles using lag cells 0.1 mm wide. An example covariance plot is given in figure B-5, which displays the results as complement covariance (i.e., variance minus covariance) and resembles a traditional variogram. The covariance estimates obtained from the detrended elevation data provided paired values that could be analyzed with the matched-pairs t-test discussed earlier. Results of the t-tests (table B-6) indicated that roughness data collected by the profilometer and the stereo digitizer had similar covariances. Differences in the matched covariance values were caused primarily by differences in variances.

Table B-5.—Sample variances and calculated two-sample F-statistics for roughness data obtained by mechanical profilometer (MP) and stereo digitizer (SD), square millimeters

Profile	Raw data			Detrended data		
	MP var	SD var	F-value	MP var	SD var	F-value
x-DIRECTION						
1	0.5367	0.4821	1.113	0.1912	0.1871	1.022
2	1.9468	1.8032	1.080	.4687	.4430	1.058
3	1.6388	1.4550	1.126	.2444	.2246	1.088
4	.3695	.3239	1.141	.2553	.2342	1.090
y-DIRECTION						
5	0.5313	0.5696	1.072	0.1642	0.1579	1.040
6	.5209	.5505	1.057	.0929	.0803	1.157
7	.2994	.2699	1.109	.0637	.0597	1.067
8	2.7014	2.3481	1.150	.1267	.1375	1.085

var Variance.

Table B-6.—Comparative roughness measures for rock fracture profiles obtained by mechanical profilometer (MP) and stereo digitizer (SD)

Profile	Estimated JRC		Covariance matched pairs		C(O) profile length		Fractal dimension	
			Calculated	Probability				
	MP	SD	t-statistic		MP	SD	MP	SD
1	10	11	-1.39	0.172	0.0032	0.0032	1.262	1.120
2	19	18	-.17	.866	.0079	.0075	1.145	1.074
3	13	12	-.33	.745	.0041	.0038	1.194	1.071
4	12	11	-.95	.346	.0043	.0040	1.140	1.058
5	7	4	-1.16	.253	.0025	.0024	1.275	1.091
6	6	2	.06	.950	.0013	.0011	1.269	1.114
7	2	1	-.39	.696	.0009	.0008	1.223	1.094
8	10	9	.72	.478	.0022	.0024	1.229	1.123

C(O) Covariance of estimator.
JRC Estimated joint roughness coefficient.

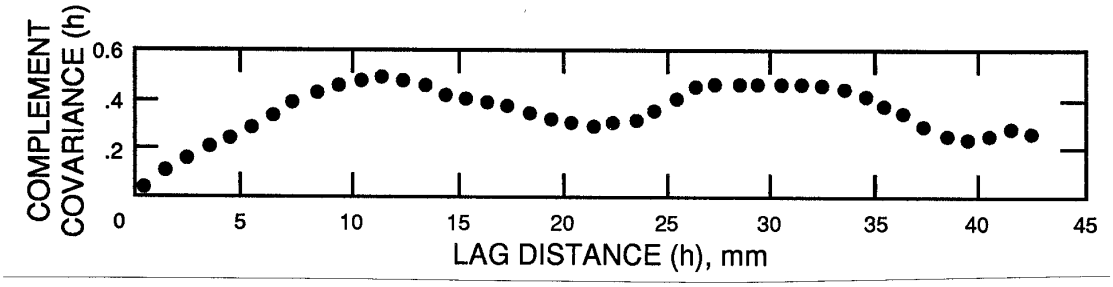

Figure B-5.—Complement covariance plot for elevations measured along profile 4 using mechanical profilometer. (Number of data points = 1,161; width of lag cells = 0.1 mm; sample mean = 0.5 mm; and sample variance = 0.3695 mm^2). (h = separation distance or lag.)

Another means of comparing the results of the two profiling methods was based on the Yxx(0) parameter proposed by Wu and Ali (*47*). In this scheme, Yxx(0) is equal to the covariance of estimation [C(O)] divided by profile length; smooth fractures are those with Yxx(0) less than 0.2. As shown in table B-6, there was excellent agreement between the two methods. The small values seemingly indicated a fairly smooth fracture surface, but based on experience, the investigators do not agree with Wu and Ali's criterion.

The final comparison was the fractal dimension, which is a measure of how much a surface profile fills its topological space (*10*, *32*). Most rock fracture profiles have fractal dimensions between 1.0 and 1.5, where a higher number indicates a rougher surface. Using the criteria suggested by Brown (*12*), the fractal dimension of each profile was calculated by the divider method, taking care to magnify the elevation values sufficiently to avoid underestimating the fractal dimension. These computed fractal dimensions are presented in table 1. The fractal dimensions calculated using the stereo digitizer were approximately 10 pct less than those obtained from the profilometer, which indicated that (1) some smoothing was invoked on the roughness data during the photogrammetric and stereo-digitizing procedures and/or (2) the profilometer method had some random noise induced by variability in electrical current during voltage readings or by differences in rock hardness.

The differences in paired fractal dimensions also suggested that the fractal dimensions were quite dependent on the finest available scales of measurement. This notion was verified by computing the fractal dimensions of profilometer profiles smoothed by a three-point, moving-window averaging scheme; this scheme typically reduced the calculated fractal dimension by 1 to 5 pct. Further evidence for the importance of the digitizing increment was shown by the relatively small fractal dimensions of profiles 2, 3, and 4. Earlier studies, where the first four traces (x-direction) were rougher than the last four traces (y-direction), indicated anistropy in surface roughness.

Therefore, in this study, the evidence suggests that the fractal dimension may not be the same type of roughness measure as that used by other investigators. It appears that fractal dimensions may be influenced heavily by short wavelength components of a fracture surface, whereas variance-based and Z_2-type parameters may depend more on longer wavelength components. More research is planned to investigate such relationships.

Conclusions on Comparing Photogrammetry and Profilometers

Close-range photogrammetry and stereo digitizing provided a means to measure rock fracture roughness. With the capabilities of current equipment, stereo digitizing had slightly poorer resolution in the horizontal plane and slightly less accurate repeatability in the vertical plane than mechanical profilometers when laboratory-scale rock specimens were examined.

Five statistical comparisons and four derived roughness measures (visual, JRC, Yxx(0), and fractal dimension) were used to compare close-range photogrammetry and stereo digitizing as methods of measuring rock fracture roughness. Of the nine comparison criteria, seven indicated no significant difference between the techniques. Thus, reasonable compatibility between profilometer methods and stereo-digitizing methods has been established.